TECTONICS, VOL. 10, NO. 2, PAGES 433-453, APRIL 1991

EARTHQUAKES AND OPHIOLITE EMPLACEMENT IN THE MOLUCCA SEA COLLISION ZONE, INDONESIA

Robert McCaffrey

Department of Geology, Rensselaer Polytechnic Institute, Troy, New York

Abstract. The Molucca Sea in eastern Indonesia is the site of an active arc-arc collision, and among its interesting features is the exposure of ophiolitic rocks on islands of the Talaud-Mayu Ridge (TMR), a largely submarine ridge formed of highly deformed rocks that bisects the collision zone. To explore the relationship between earthquakes and uplift of the ophiolite, the centroid depths and fault plane solutions of 18 large earthquakes occurring in the past 20 years beneath the TMR are constrained by inversion of their teleseismic, long-period P and SH waveforms. Centroid depths range from 16 to 36 km, but uncertainties allow a range of 10 to 45 km. All events show thrust faulting; nodal planes strike parallel to the NNE trending TMR and dip 40±9° to the ESE and 53±9° to the WNW. Published seismic refraction and gravity data support the inference that the WNW dipping, steeper nodal planes are the fault planes. Dips do not change with depth, indicating either that the fault flattens below 40 km depth or that the steeply dipping fault penetrates the entire thickness of the lithosphere. I conclude that the Molucca Sea ophiolite is being lifted by high-angle thrust faults (45° to 60°) that extend at least 15 km into the upper mantle. Summing seismic moment tensors and assuming uniformly distributed deformation suggest that the closure across the Molucca Sea collision zone may account for 14% to 59% of the Pacific-Eurasia convergence vector or 15% to 63% of the Philippine-Eurasia convergence. Moment tensor sums provide estimates of crustal thickening rates beneath the TMR of 7 to 20 mm/yr and these imply uplift rates of 2 to 6 mm/yr if the increase in crustal thickness is isostatically compensated. Hence the ophiolite and an enormous volume of mélange are being lifted higher than the flanks of the island arcs and will be emplaced on them by gravity. I suggest that ophiolites occur in this tectonic setting because the concave down shape of the subducted oceanic lithosphere beneath the Molucca Sea increases its effective buoyancy, preventing it from sinking out of the way of the encroaching island arcs. This case suggests a family of convergent margin settings in which normal oceanic lithosphere is buoyed up so that ophiolites can be stripped from it and emplaced on a continental margin or island arc. These settings include those where (1) slab geometry restricts asthenospheric flow away from the convergent margin, (2) subduction of younger, less dense lithosphere decreases its negative buoyancy, (3) a passive continental margin resists subduction, or (4) the presence of a thick thermal boundary layer beneath a passive continental margin inhibits asthenospheric flow necessary to accommodate the sinking oceanic lithosphere.

Paper number 90TC02553.
0278-7407/91/90TC-02553$10.00

INTRODUCTION

Geologic structures in many of the world's mountain belts reveal complex histories involving closure of oceanic basins, ophiolite emplacement, and termination by collision between buoyant elements, such as continents or island arcs [e.g., Dewey and Bird, 1970]. Processes occurring during the final stages of basin closure determine, to a large degree, the deep structure within the ensuing mountain belt. Thus studies of modern examples of the late stages of basin closure and incipient collision can lead to an increased understanding of the structure of mountains and the processes that produced them.

A modern example of basin closure is the arc-arc collision in the Molucca Sea, Indonesia (Figure 1). Beneath the Talaud-Mayu Ridge (TMR), earthquake activity is extreme (Figure 2a) and geologic and gravity evidence indicate the presence of ophiolite, probably in the process of being emplaced onto the island arc along with an enormous volume of mélange, called the collision complex. I examine earthquake data to constrain

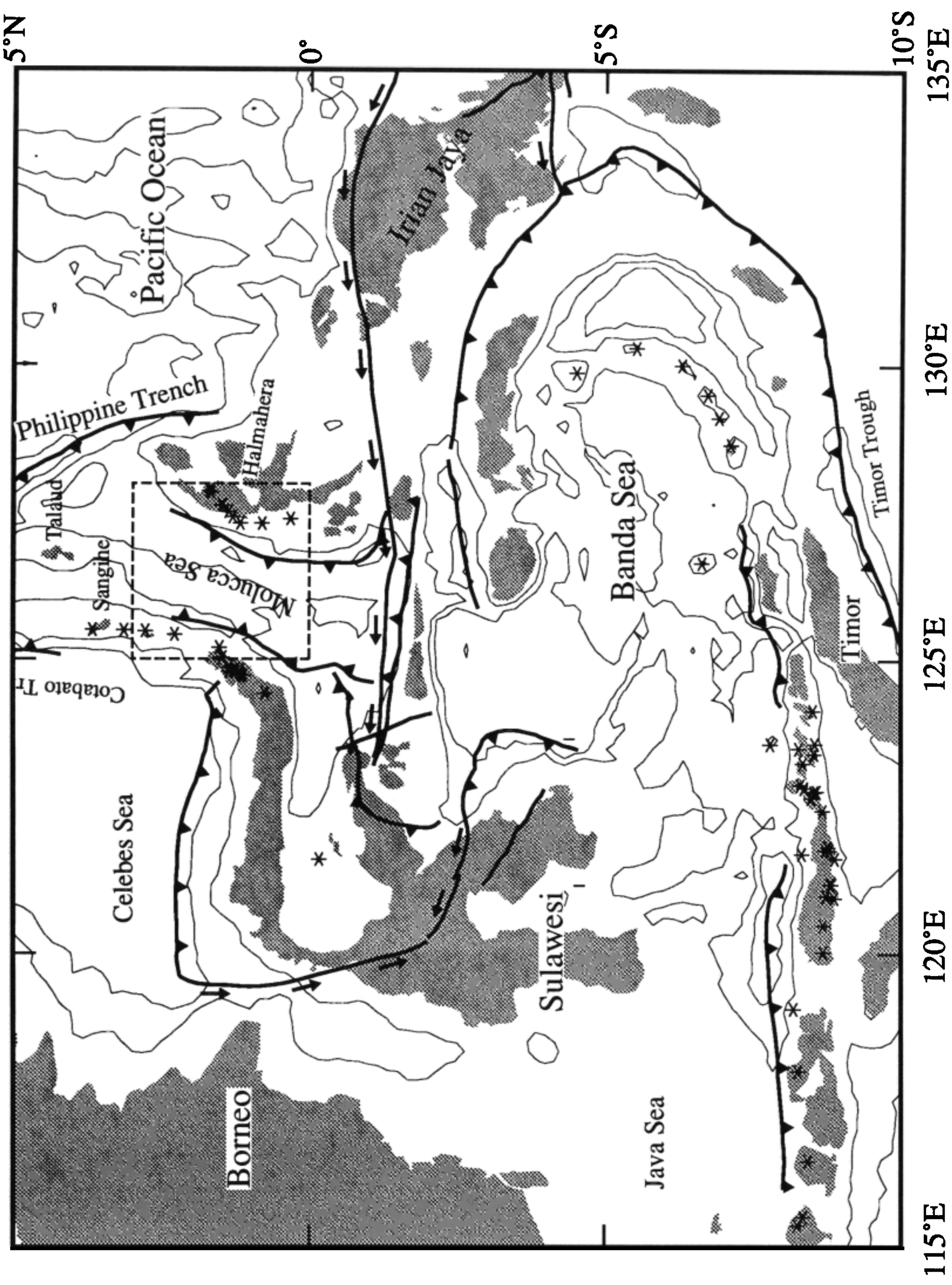

Fig. 1. Map of eastern Indonesia showing the study region enclosed in a dashed box. The Talaud-Mayu Ridge extends from Talaud Island southward through the central Molucca Sea. Asterisks indicate positions of volcanoes, and bathymetry is contoured every 2000 m. Arrows on strike-slip faults show the motion of one side with respect to the other.

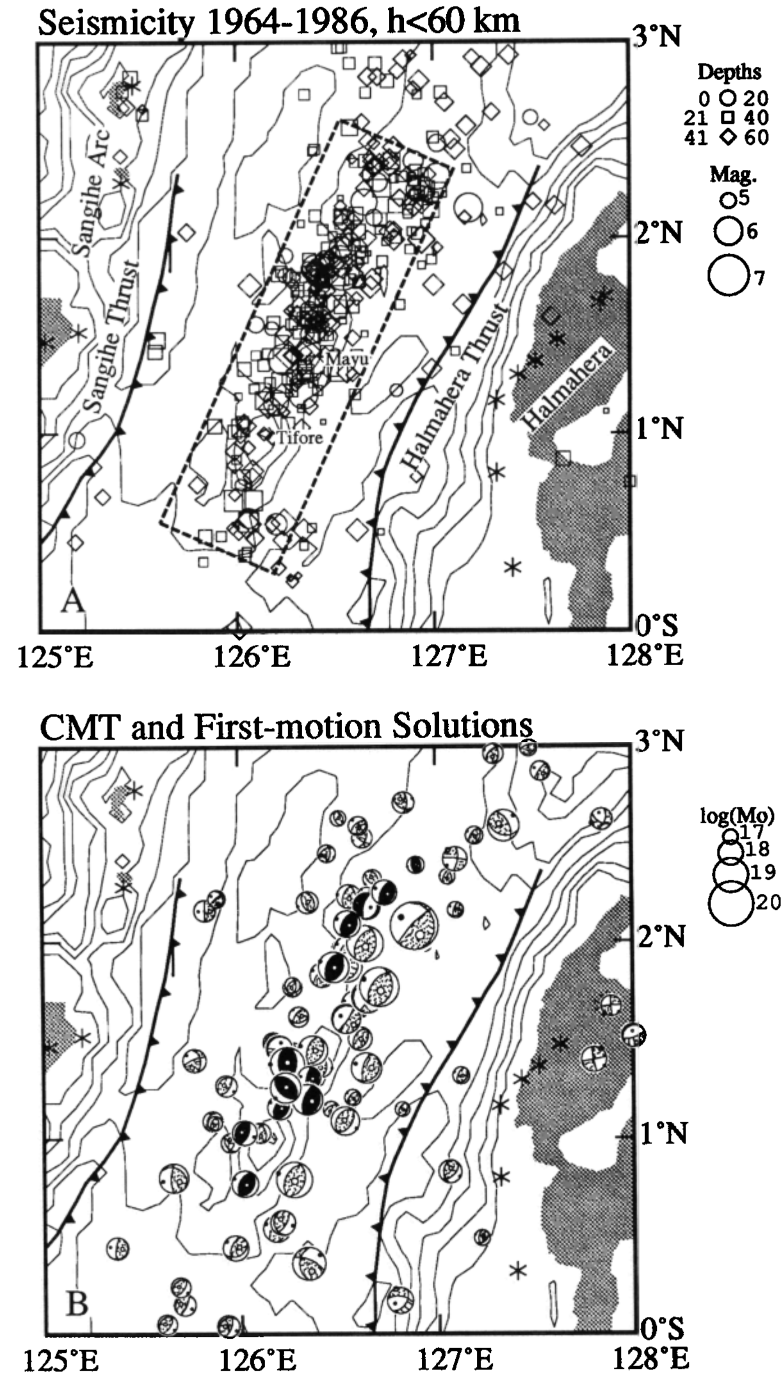

Fig. 2. (a) Map of shallow earthquake epicenters for the Molucca Sea region. Events are taken from the list of the International Seismological Centre (ISC). Shown are those with a magnitude of greater than 4.0 and with more than 15 stations used in the location. The dashed box outlines the region for which the deformation analysis is done. Asterisks indicate positions of volcanoes, and bathymetry is contoured every 500 m. (b) Fault plane solutions for earthquakes with reported depths of less than 60 km. Compressional quadrants are shaded; circles show T axes, and dots are P axes. Solutions with solid fill in compressional quadrants are based on first motions and the remainder are centroid-moment tensor (CMT) solutions. The sizes of the focal spheres are proportional to the log of the seismic moment as shown at the right. For the first-motion solutions the seismic moment is estimated from the magnitude, using equation (1).

the emplacement of the ophiolite in this arc-arc collision, that is, whether it is thrust upwards along a fault that penetrates deeply into the mantle or along a near-horizontal fault that detaches thin slivers of crust and upper mantle. In the past, such details have been masked by the poor resolving power of teleseismic earthquake arrival time data for the earthquake's depth. In this study I use long-period teleseismic P and SH waveforms to constrain centroid depths and fault plane solutions for 18 earthquakes of magnitudes greater than 5.5 that occurred in the past 20 years beneath the TMR.

Overview of the Structure and Tectonics of the Molucca Sea Collision Zone

Eastern Indonesia forms a broad zone of deformation that separates the Eurasian, Australian, and Philippine Sea plates and is a likely analog for Mesozoic terrane accretion in western North America [e.g., Silver and Smith, 1983]. The arc-arc collision in the Molucca Sea is part of the Eurasia-Philippine Sea plate boundary and juxtaposes the Sangihe volcanic arc on the west and the Halmahera arc on the east, convex towards one another and separated by a minimum distance of about 250 km (Figure 1). East of Halmahera, the Philippine trench is migrating southward, possibly foretelling a future flip in subduction direction [Cardwell et al., 1980; Hamilton, 1979; Nichols et al., 1990].

Between the volcanic arcs is the Molucca Sea, a basin with water depths that rarely exceed 2 km but underlain by an enormous volume of deformed rocks called the collision complex [Silver and Moore, 1978; McCaffrey et al., 1980]. The collision complex was recognized by Hamilton [1977, 1979] as a tectonic mélange by its chaotic character in seismic reflection profiles. Silver and Moore [1978] recognized that the collision complex is in thrust contact with the slopes of the island arcs at both the Sangihe thrust in the west and the Halmahera thrust on the eastern side (Figure 2). The thrust zones verge opposite to those of the trenches that accommodated subduction of the Molucca Sea plate beneath the island arcs (Figure 1). Silver and Moore [1978] suggested that movement of the collision complex up the island arc aprons is driven along the thrusts by gravitational flow away from the bathymetric high of the central TMR.

In the northern Molucca Sea, the Halmahera and Sangihe thrusts are not clear, and the deformation observed in the surface sediments near the Talaud Islands is negligible compared to that farther south [Cardwell et al., 1980; Moore and Silver, 1983]. In this section the Cotabato trench and the Philippine trench appear to be new features and any volcanism associated with the Sangihe and Halmahera arcs has died out. Thus the northern Molucca Sea has the appearance of being in a later stage of collision.

The collision complex is exposed on the islands of Mayu and Tifore (Figure 2a) where serpentinite, diabase, porphyrite, gabbro, and harzburgite are present. On the Talaud Islands in the northern Molucca Sea, dismembered slabs of ophiolite comprising serpentinized peridotite, gabbro, spilites, and cherts are enclosed in a scaly clay matrix and thrust over Tertiary sedimentary rocks [Moore et al., 1981; Sukamto, 1979]. Field relations suggest that the ophiolite on the Talaud Islands is Eocene or older oceanic crust and upper mantle emplaced along east dipping faults during the Miocene [Moore et al., 1981].

Ophiolites are also exposed farther north on the Pujada Peninsula of southeast Mindanao where they are overlain by and incorporated into mid Miocene to Pliocene conglomerates indicating a pre-mid Miocene emplacement [Hawkins et al., 1981]. To the south is a large ultramafic body on Sulawesi with a nearly complete smaller ophiolite exposed on the East Arm [Silver et al., 1983]. Thus the collision is producing a belt of ophiolites that in the end will mark the suture between the two island arcs and possibly be surrounded by mélange. Such relations are inferred in the Sierra Nevada in California and may be indicative of a mid Jurassic arc-arc collision there [Schweickert and Cowan, 1975; Moores and Day, 1984].

A high in the gravity field over the TMR from about 2°N to 0.5°N requires the presence of a large mass more dense than the deformed collision complex to comprise the TMR at least in part. The exposures of mafic and ultramafic rocks on Mayu and Tifore imply that oceanic crust forms this root. McCaffrey et al. [1980] present two seismic refraction profiles separated by 50 km that reveal the collision complex west of the TMR to be about 4 km thinner than it is to the east. Thus refraction results and the asymmetry in the gravity field suggest that basement is offset beneath the TMR. This same region is extremely active seismically and is characterized by large earthquakes with reverse faulting mechanisms (Figure 2b).

Teleseismic Waveform Analysis

The goal here is to constrain the depths and fault plane solutions of large earthquakes beneath the Talaud-Mayu Ridge (TMR) well enough to understand the style of deformation beneath the TMR. Waveforms recorded at teleseismic distances of 30° to 90° are suited for this purpose because they contain information about the source but are effected in a predictable manner by propagation through the Earth. Such waveforms are strongly influenced by the orientations of the fault plane and slip direction, the depth of the source, crustal structure, and the slip history on the fault. At long wavelengths, details of the slip history and crustal structure are smoothed so that the long-period waveforms are excellent for the estimation of nodal plane orientations and depths of earthquakes.

The waveform inversion method used is that of McCaffrey et al. [1991], which is based on Nabelek [1984], Helmberger [1974], and Langston and Helmberger [1975]. Long-period teleseismic body waves from the World-Wide Standardized Seismograph Network (WWSSN) were hand digitized, and seismograms from the Global Digital Seismic Network (GDSN) were obtained. Typically, 10 to 30 seismograms are available for each event (Table 1). The double-couple point source is described by the strike and dip of one of the nodal planes, the rake angle on that surface [Aki and Richards, 1980], the centroid depth, and the amplitudes of overlapping isosceles triangles comprising the source time function [Nabelek, 1985]. The inversion routine finds the set of parameters that minimizes the weighted sum of the squares of the residuals between the amplitudes of the observed and calculated seismograms. Figure 3 shows four examples of waveforms and their solutions.

The statistical uncertainties in the source parameters estimated by the inversion routine are much less than the uncertainties that one would estimate by testing how much a parameter can be varied without visibly violating the observed waveform shapes

TABLE 1. Summary of Fault Plane Solutions

	Date	Origin Time, UCT	Latitude, °N	Longitude, °E	Depth, km	m_b	Moment, 10^{16} Nm	Dur., s	Strike, deg	Dip, deg	Rake, deg	N. P. 2 ϕ	N. P. 2 δ	P Axis Az	P Axis Pl	T Axis Az	T Axis Pl	B Axis Az	B Axis Pl	Pw	Sw	Pg	Sg
1	66 3 8[1]	541:02.8[2]	1.87	126.43	19.1± 5.3	5.8	248± 21	7.6	31±10	47±3	88± 7	213	43	122	2	269	87	32	1	14	7	0	0
-	66 810	2 7:00.0	1.38	126.24	25.4± 6.5	6.3	50000±2775	29.	24±26	32±3	80±16	215	59	301	13	143	75	32	5	8	0	0	0
2	68 817	400:35.0	1.32	126.34	20.8± 6.8	5.7	185± 19	3.3	202±10	62±5	96±11	10	29	288	17	125	72	19	5	19	9	0	0
3	681031	906:34.9	1.20	126.36	20.0± 6.4	6.1	163± 17	2.2	188±11	61±5	95±11	358	30	275	16	112	74	6	5	17	12	0	0
4	69 125	519:17.4	0.74	126.02	24.5± 6.8	5.9	177± 15	6.9	20±10	43±3	92± 9	198	47	289	2	74	88	199	1	13	11	0	0
5	69 8 5	213:10.2	1.22	126.23	35.7± 9.0	6.1	6501±342	17.1	355± 9	49±2	81± 7	189	42	92	3	205	82	1	7	15	4	0	0
6	70 8 8	2104:05.8	1.20	126.26	15.8± 6.6	5.8	74± 6	5.1	201±12	46±4	76±11	40	45	301	0	33	80	211	10	13	8	0	0
7	73 318	1106:15.4	2.09	126.57	35.7± 8.6	5.9	1052± 78	11.1	349±14	38±3	74±11	188	54	270	8	139	77	1	9	17	5	0	0
8	73 5 4	1127:13.8	2.25	126.74	33.1±14.3	5.8	85± 12	7.1	207±12	63±6	83±13	43	28	302	17	100	71	210	7	11	8	0	0
9	74 5 9	1327:39.0	0.83	126.07	26.2±18.6	5.6	57± 11	6.3	200±18	55±8	77±17	42	37	299	9	68	76	208	11	6	5	0	0
10	74 511	043:45.3	1.88	126.47	35.6± 7.4	6.1	239± 17	3.3	22±13	39±3	90± 9	202	51	292	6	111	84	202	0	16	8	0	0
11	75 513	2118:40.3	1.05	125.99	21.2± 3.9	5.8	791± 47	12.2	21± 5	55±2	91± 5	199	35	110	10	294	80	200	1	15	5	0	0
12	77 7 3	1439:11.4	1.43	126.37	23.0± 6.0	6.0	262± 23	3.2	190±13	50±4	100±11	355	41	273	4	154	81	4	7	11	6	0	0
13	781214	1925:56.7	0.55	126.08	33.1±14.3	6.0	75± 9	4.1	208±11	68±7	114±13	338	32	280	20	152	60	18	22	8	4	0	0
14	791022	558:48.4	0.67	126.02	27.8± 8.8	6.2	672± 57	8.7	173±10	58±4	98± 9	338	33	257	13	106	75	349	7	16	8	0	0
15	84 723	1603:39.3	1.37	126.44	22.6± 9.7	5.8	210± 24	6.1	189±15	62±7	87±14	14	28	281	17	92	73	190	2	11	7	6	4
16	841026	849:20.3	1.68	126.36	17.5± 6.6	5.8	175± 13	7.8	234±11	52±4	113± 8	20	44	308	4	205	72	40	18	13	6	3	4
17	85 413	300:06.8	1.62	126.41	23.4± 5.8	6.4	4221±266	21.3	12± 5	39±1	78± 4	207	52	291	7	158	80	22	7	9	3	7	6

Uncertainties are 10σ for depth, 5σ for strike, dip, and rake, and 2σ for seismic moment where σ is the statistical standard error. Origin times and epicenters have been recalculated for the revised depths (except for the 1968.8.10 event). Duration (Dur.) is the time during which 95% of the moment was released. N.P. 2 gives the strike ϕ and dip δ of the second nodal plane. Pw, Sw, Pg, and Sg are the numbers of P and S waveforms from the WWSSN and the numbers of P and S waveforms from the GDSN, respectively. Az and Pl are abbreviations for azimuth and plunge of the axes.

[1] Read as March 8, 1966.

[2] Read as 5 hours, 41 minutes, and 2.8 seconds.

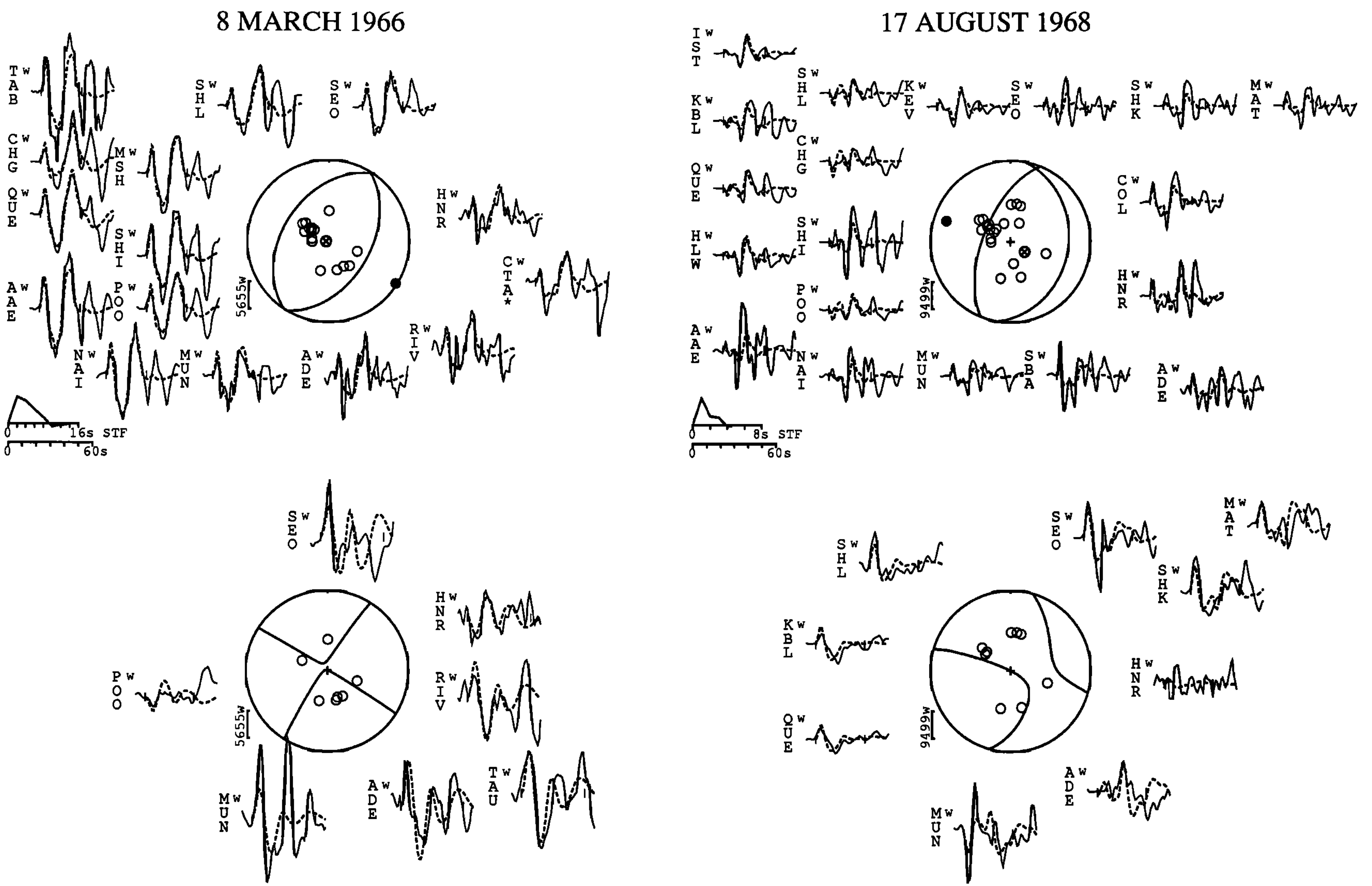

Fig. 3. Examples of waveforms and solutions for Molucca Sea earthquakes. In each plot, at the top, P waveforms surround the focal sphere, while the ray intersections and P radiation pattern nodes are shown in the lower hemisphere projection. At the bottom is the same format for the SH. Observed seismograms are shown by continuous traces, and synthetic seismograms are shown by dashed lines. The station codes are written vertically, and the small letters near the station codes and amplitude axes identify WWSSN (w) and GDSN (d). Vertical bars bracket the part of the trace used to constrain the source parameters in the inversion, and an asterisk below the station code indicates that the seismogram

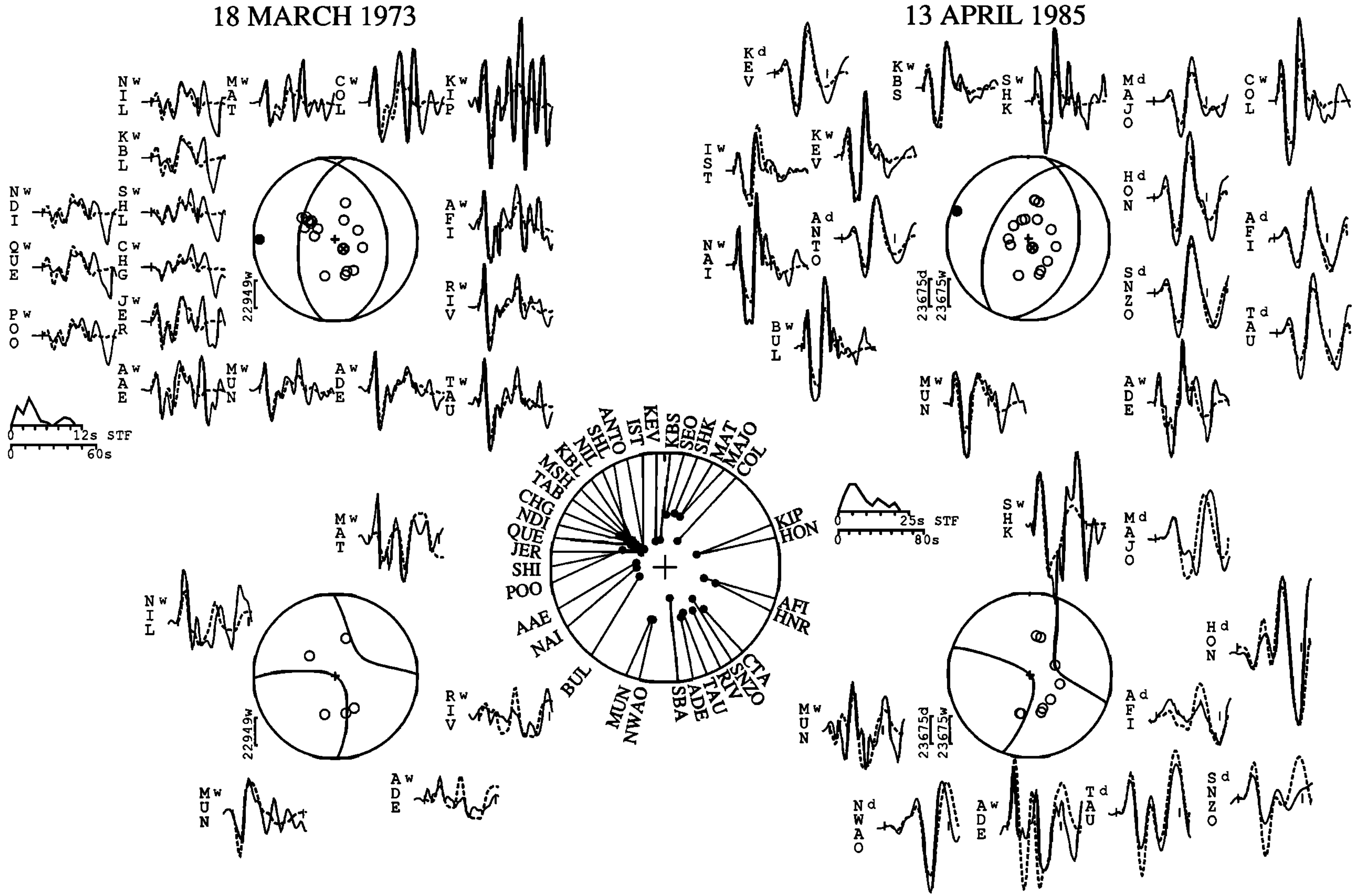

Fig. 3. (continued)
was excluded from the inversion. Seismogram amplitudes correspond to a common instrument magnification (3000) and epicentral distance (40°) so that the variations among them are preserved (the amplitude scale at the lower left of each focal sphere is labeled in microns). P axes are shown by solid circles and T axes by ⊕. Two time axes are shown for each event, one for the seismograms and the other for the normalized source time function (labeled STF). The inset shows the positions of the stations on the lower focal hemisphere.

[e.g., McCaffrey and Nabelek, 1986, 1987; McCaffrey, 1988; Nabelek, 1984; Stein and Wiens, 1986]. Uncertainties estimated by the above process are typically ±5 km in depth, ±15° in strike, ±5° in dip, and ±20° in the rake angle. Statistical errors of 2σ for seismic moment, 10σ for depth, and 5σ for the strike, dip, and rake angles, where σ is the standard error given by the inversion routine, approach the error estimates found by testing each parameter [Nabelek, 1984] and are the basis for those given in Table 1.

Crustal Structure

Seismic refraction profiles are used to constrain the source structure needed for the generation of the waveforms [McCaffrey et al., 1980]. In particular, profile 10-5 is above the region of earthquake activity, and 10-4 is about 50 km to the east (Figures 4 and 5). Both profiles show basement with seismic velocities of 6.5 to 7.0 km/s that correspond to oceanic crustal layer 3 (presumably oceanic crust underlies the collision complex). The average thickness for layer 3 is 5 km [Christensen and Salisbury, 1975] so it is likely that the Moho is near 16 km depth beneath 10-5 and near 20 km depth beneath 10-4 (Moho arrivals were not observed in the refraction profiles).

Because the earthquakes examined here occurred beneath the TMR, below which there may be an offset in basement, the seismic rays that travel to stations to the east and west likely sample different structures. The 4 km difference in thickness of the collision complex layer between 10-5 and 10-4 (Figure 4) will produce about a 1.5 s delay in the upgoing pP and 2.5 s delay in the upgoing sS for the eastern stations with respect to those to the west. Tests with synthetic seismograms indicate that a delay of this magnitude would be observable in WWSSN seismograms (a clear example of azimuthal variations in delay times is given by Nelson et al. [1987]). However, the Molucca Sea seismograms do not display this delay, and the incorporation of separate source structures for the eastern and western stations did not improve the visual fits or significantly decrease the residual variance. Possibly the seismic velocity at the base of the collision complex is close to that of the upper part of the oceanic crust. Due to the lack of a noticeable difference in the observed seismograms with azimuth, the same source structure consisting of horizontal plane layers was used for generating synthetic seismograms at all azimuths and was taken as the average of the profiles 10-5 and 10-4 (Figure 4).

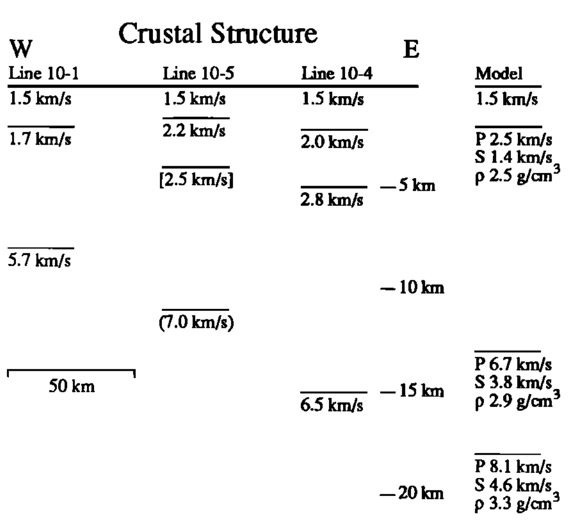

Fig. 4. Crustal structure on a line across the Molucca Sea reported from seismic refraction profiles shown in Figure 5a. P wave seismic velocities are given for each layer, where those in brackets are assumed velocities and those in parentheses are apparent velocities for unreversed profiles [McCaffrey et al., 1980]. At the right is the average layered structure used for the generation of synthetic seismograms. Shown are the P and S velocities and the densities (ρ) assumed.

In some instances the waveforms are sensitive to the source velocity assumed because an increase in it moves the takeoff angles away from the vertical and toward the nodal planes of these thrust earthquakes. For example (Figure 6), the beginning of the seismograms for stations that fall close to the nodal planes for the event of 8 March 1966 match the initial pulse better when a crustal source velocity is used, while others, such as those for the event of 17 August 1968, give a better match with a mantle velocity. The depths of the earthquakes along with their constraints on the source velocity suggest that the Moho is at about 20 km depth.

RESULTS

Results of Waveform Analysis

The earthquake parameters of most interest in this study are the source depths and the dips of the nodal planes. Most of the events are nearly pure thrust and strike parallel to the TMR so that the nodal planes dip to the ESE and WNW (Figure 5a). Minimum variance depths are 15 to 36 km, and reasonable bounds are 10 to 45 km, so these events likely fall within the crust and uppermost mantle. This depth range is similar to that found for microearthquakes in the region [McCaffrey, 1982].

In Figure 5b the earthquake mechanisms are superimposed on a crustal model constrained by seismic refraction and gravity data [McCaffrey et al., 1980]. The high-density slab beneath the TMR is required by gravity values that are high over the ridge and cannot be explained by the topography of the low-density ridge alone. Gravity observations, however, cannot usefully constrain the attitude of the high-density mass.

Both gravity and seismic refraction observations indicate that the basement beneath the collision complex is a few kilometers shallower on the west side of the TMR than it is on the east side. If thrusting caused this offset in basement, then the west dipping nodal planes are the fault planes. It is possible that the earthquakes show only the latest stage of the collision and are unrelated to the present structure, in which case one cannot use the basement offset to infer the modern sense of thrusting. Nevertheless, because all nodal planes dip fairly steeply (≥30°), the possibility of an east dip changes only the specific interpretation of the emplacement direction and not the general conclusion of emplacement along a steep fault.

The positions of the earthquakes directly beneath the TMR and their steep nodal planes suggest that the faults along which the oceanic crust is thrust are steeper than the inclination of the slab shown in Figure 5b. The plot of dip angles versus strike angles (Figure 7a) suggests that the west dipping nodal planes dip more steeply than the east dipping planes although there is a large overlap in the distributions. However, all dips are quite high (30° to 60°), demonstrating that the structure being lifted is a thick block rather than a thin sheet. Neither plane demonstrates a change of dip with depth (Figures 7b and 7c) so that if the fault zone turns to a shallow dip, it does so below 40 km depth. Otherwise the fault may cut the entire lithosphere.

Earthquake of 10 August 1968

Two earthquakes in the Molucca Sea have seismic moments of greater than 10^{20} N m and hence dominate the moment tensor summations below. The 14 August 1986 event has a centroid-moment tensor solution (CMT [Dziewonski et al., 1981]) that is atypical of Molucca Sea earthquakes (the largest focal sphere in Figure 2b) and M_o of 2.26×10^{20} N m. In general, the CMT double-couple solutions are very similar to body waveform solutions and the moment estimates agree to within 10-20% [Abers, 1989; Ekström and Dziewonski, 1988; McCaffrey, 1988], so I use CMT solutions for this and other earthquakes without body waveform solutions.

For the other large earthquake (10 August 1968) that occurred prior to operation of the GDSN, P waves were off scale on the analog WWSSN records, but I was able to find 11 P_{dif} arrivals (P waves that are diffracted at the core-mantle boundary). Because direct determination of the seismic moment with P_{dif} is unreliable, I first estimate moment by comparing the P_{dif} amplitudes for the 1968 event to those of the 5 August 1969 event (Table 1), which had a similar fault plane solution and a seismic moment estimated from P and SH waveforms. The average ratio of the amplitudes (1968/1969) is 5.2 with a range of 4.3 to 7.1 (Figure 8) so that direct comparison of the amplitudes suggests that the 1968 event has a moment ranging from 2.8 to 4.6 $\times 10^{20}$ N m. However, if the source duration of the 1968 event was much larger than that of the 1969 event, then this may underestimate the moment of the 1968 earthquake.

A second, perhaps better, approach to estimate the moment of the 1968 event is to use the 1969 event to estimate the bias in moment that arises from using P_{dif} waveforms. In doing this I model P_{dif} as a P wave and extrapolate the P geometrical spreading curve of Langston and Helmberger [1976] to distances greater than 90°. Eight P_{dif} seismograms (at distances of 102° to 121°) for the 1969 earthquake were inverted for two cases, one with the double couple fixed at the minimum variance solution found with the P and SH waves and a second with the mechanism free to change. Both cases yielded a moment of 1.88 $\times 10^{19}$ N m, or 3.5x smaller than the moment determined with P and SH waves. The reduction in moment of 3.5x in modeling P_{dif} as P waves is similar to that found by McCaffrey and Nabelek [1986] for an earthquake north of Timor, suggesting that the factor may not be very sensitive to the specific seismograms used.

The minimum variance mechanism for the 1968 event (Figure 9a), using P_{dif} seismograms recorded at the same stations, is a NNE striking thrust similar to the majority of events in the region. Residual variance is least at a depth of 25 km, a duration of 40 s, and an apparent moment of 4.29×10^{20} N m. This event likely ruptured the entire thickness of the seismogenic layer.

Because the calculated seismic moment depends strongly on the assumed source centroid depth, the 1968 event was modeled at several depths to constrain the range of possible depths and seismic moments for it (Figure 9b). Sources deeper than 40 km have a variance increase of 60% or more with respect to the source at 25 km suggesting that the centroid is less than 40 km depth, although this increase in misfit to the seismograms is not clear to the eye (Figure 9b). For a source centroid between 20 and 40 km the P_{dif} moment is between 2.5 and 5.0×10^{20} N m. Assuming that the bias in the moment arising from the use of P_{dif} is similar to that for the 1969.8.5 event (i.e., reduced by 3.5x) then the actual seismic moment for the 1968 earthquake, by this analysis, is 8.7 to 17.5×10^{20} N m. In the following discussion I assign a value of 5×10^{20} N m for the moment of this event with a factor of 2 uncertainty.

Estimates of Closure Rate and Uplift Rate

In this section I estimate seismic deformation rates from the seismic moments and fault plane solutions of earthquakes for the years 1964 through 1988 within the region shown by the box in Figure 2a. The box encloses the majority of the seismic activity, is parallel to the TMR, and its long dimension is nearly perpendicular to the direction of convergence of the Philippine and Eurasian plates. The northern and southern ends of the box coincide with lateral changes in several observed features of the local tectonics, such as the gravity field, bathymetry, and seismicity [McCaffrey, 1982].

Within the study area the ISC places some events at depths greater than 100 km and some CMT depths are 50 to 70 km. Both this study and a microearthquake network with seismograph stations on the TMR [McCaffrey, 1982] suggest that earthquakes occur no deeper than 40 km. Bearing in mind that the ISC depths can be greatly in error because of the lack of nearby seismograph stations and that the CMT depths can have tens of kilometers uncertainty, in the following analysis I include all events within the map region of the box and presume that they all occur within 40 km of the surface. This point is important for the strain analysis in that 40 km is used as the bottom of the seismogenic region, although it is extended to 50 km for estimates of uncertainties. Earthquakes do not appear to occur within the collision complex above 15 km depth so that the seismogenic region appears to be the 25 km of crust and upper mantle only.

First I estimate the total seismic moment for the region to show that the amount contributed by small earthquakes for which there are no fault plane solutions is insignificant. Using the calculated values of seismic moment from the waveform and CMT solutions and the body wave magnitudes m_b provided by the ISC, the relationship for M_o-m_b by linear regression is

$$\log (M_o) = 1.95\, m_b + 6.87 \pm 0.41 \qquad (1)$$

The uncertainty of 0.41 magnitude orders in M_o corresponds to an uncertainty in m_b of 0.2 units. This relationship saturates at m_b of about 6.0 so is used to estimate the seismic moments from the magnitudes of only earthquakes smaller than 6.0. Using (1), the total moment of recorded events of $m_b<6.0$ in the TMR region is 4.6×10^{19} N m with a range derived from the uncertainty above of 1.8 to 12×10^{19} N m. To estimate the total

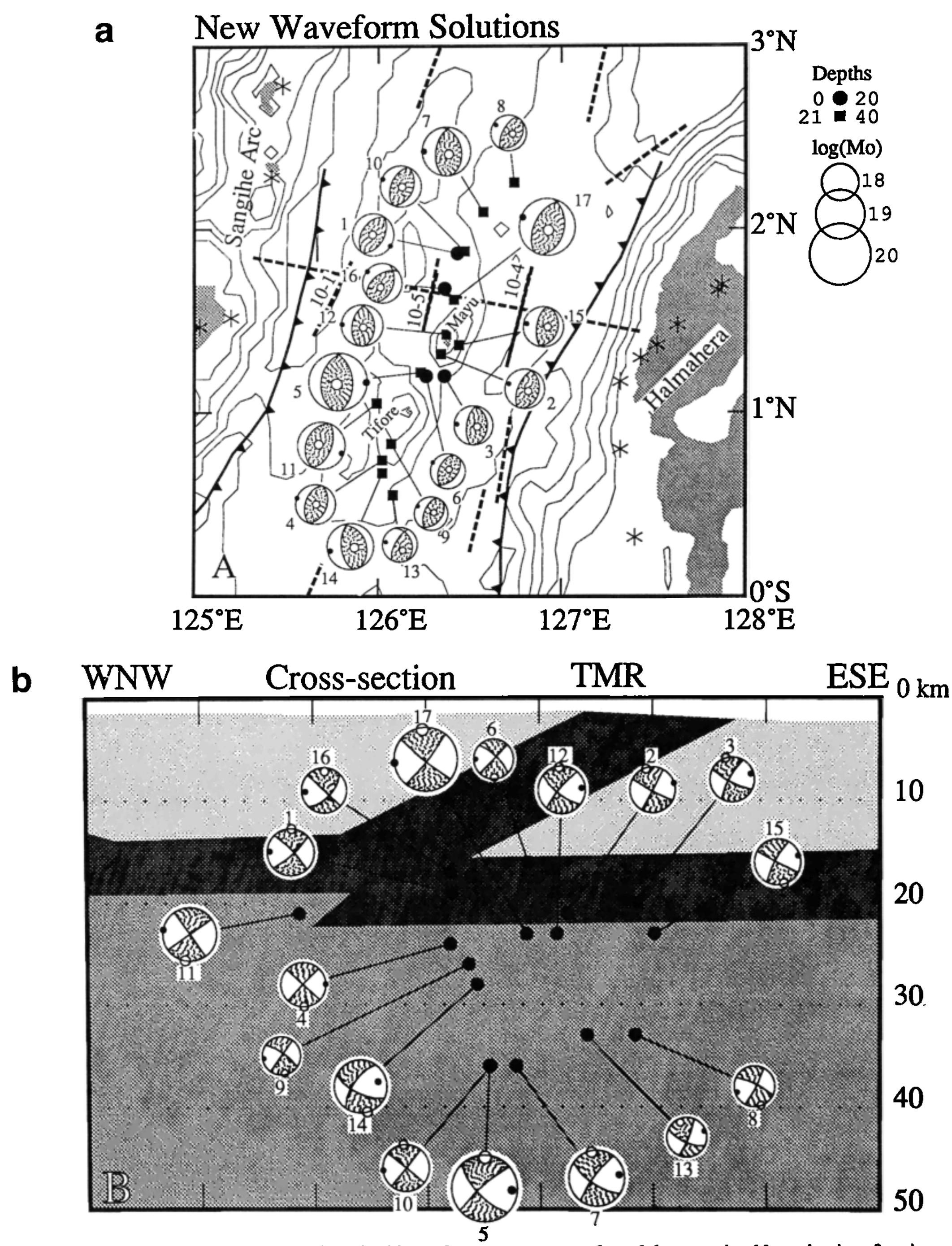

Fig. 5. (a) New fault plane solutions determined in this study. The 10 August 1968 event is not shown here. The radius of the focal sphere is proportional to the log of the seismic moment. Events are numbered as in Table 1 and plotted at the positions found by relocating with depths fixed at the values determined by the waveform analysis. The short dashed lines show the positions of seismic refraction profiles [McCaffrey et al., 1980] and the longer WNW trending dashed line gives the orientation of the cross section of Figure 5b. Asterisks indicate positions of volcanoes, and bathymetry is contoured every 500 m. (b) Cross section of the earthquake fault plane solutions superimposed on a crustal model constrained by seismic refraction and gravity data [McCaffrey et al., 1980]. The profile is centered at 1.65°N, 126.38°E and with an azimuth of 110°. No vertical exaggeration (tics at top and bottom are 0.1° or 11.1 km apart). The white area is water, light stippling represents collision complex material, slightly darker stippling represents the mantle, and the darkest represents oceanic crust. The upthrust oceanic crust may include some portion of the mantle; gravity data are insensitive to such detail. The earthquakes suggest that the high-density root may have a steeper inclination than that inferred from gravity data.

moment of unreported events, the relationship between log of N, the number of events of a given magnitude, and m_b is assumed to be linear. Again using the events of the ISC catalog for 23 years (1964-1986) we get

$$\log(N) = -1.18m_b + 7.79 \pm 0.10 \qquad (2)$$

The regression included magnitudes between 4.9 and 5.9 where the log(N)-m_b plot showed linearity, and the sampling interval for m_b was 0.1 units. Multiplying $M_o(m_b)$ found from (1) with $N(m_b)$ from (2) and summing over m_b up to 5.9, the expected total moment of Molucca Sea earthquakes for 1964-1986 with m_b<6.0 is 9.8×10^{19} N m, about double the observed value. (The range based on the uncertainties above is 3.0×10^{19} N m to 3.2×10^{20} N m.) Fault plane solutions are available for earthquakes whose moments sum to roughly half of this mean.

During 1964-1988 there were 16 earthquakes of $m_b \geq 6.0$, and we have direct estimates of moment, either by waveform analysis or CMT solutions, for all but the following four. The 11 August 1969 (23:52; m_b=6.0) earthquake was in the coda of a large Kurile Islands event but had small-amplitude seismograms so was probably no more than 10^{18} N m. A second event on 10 August 1968 (05:51, m_b=6.1) was in the coda of the large first event and by visual inspection of waveforms its moment is estimated at 5×10^{18} N m. The event of 14 December 1969 (02:42; m_b=6.0) is assigned a moment of 3×10^{18} N m from preliminary waveform modeling. The event of 18 May 1979 (23:22; m_b=6.0) has long-period vertical P waves on WWSSN

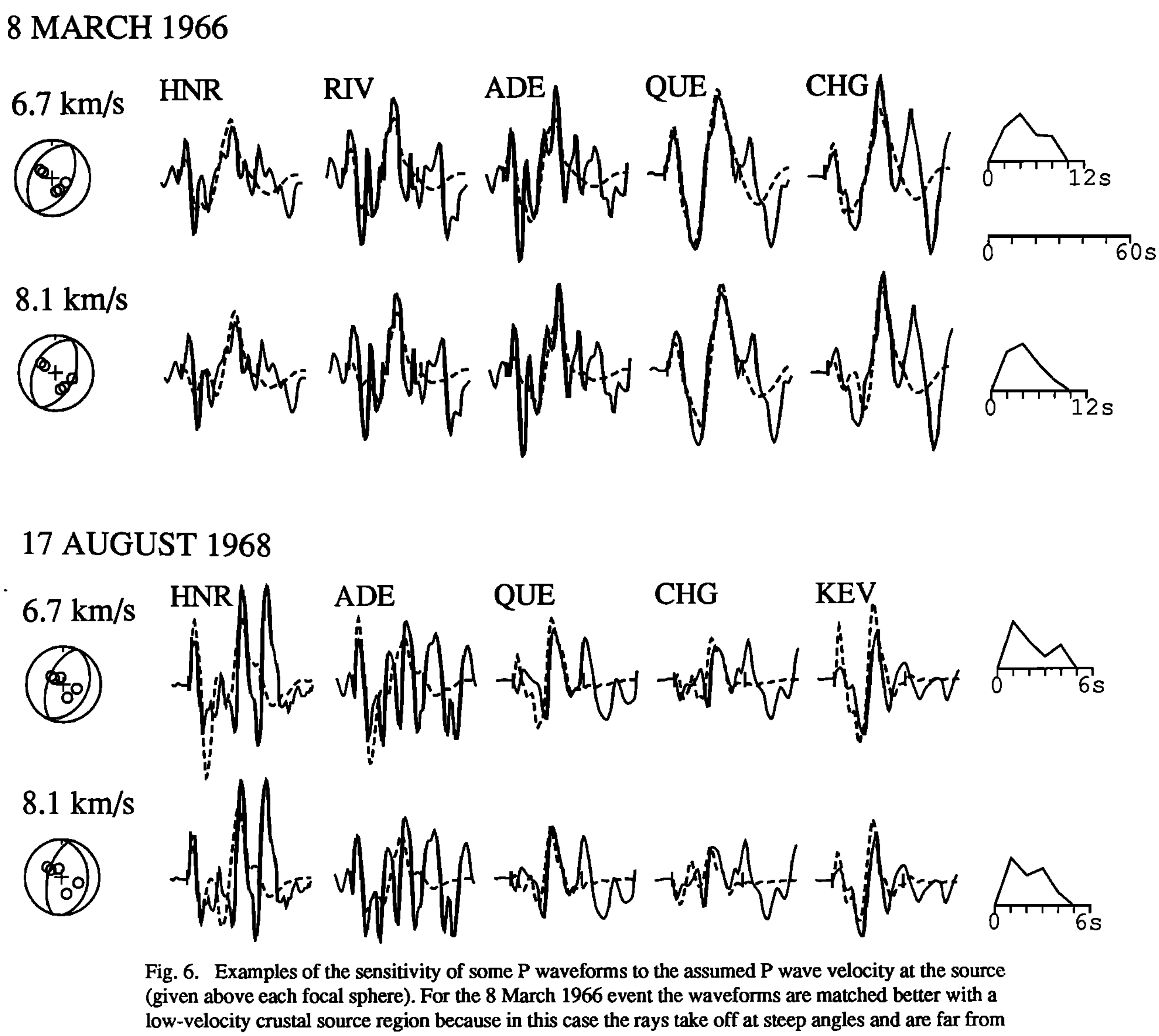

Fig. 6. Examples of the sensitivity of some P waveforms to the assumed P wave velocity at the source (given above each focal sphere). For the 8 March 1966 event the waveforms are matched better with a low-velocity crustal source region because in this case the rays take off at steep angles and are far from the nodal planes so that the high amplitude of the initial pulse is matched. For the high-velocity mantle source the rays take off too close to the nodal planes and hence are too small. For the 17 August 1968 event the opposite is true; the waveforms fit better for a high velocity in the source region.

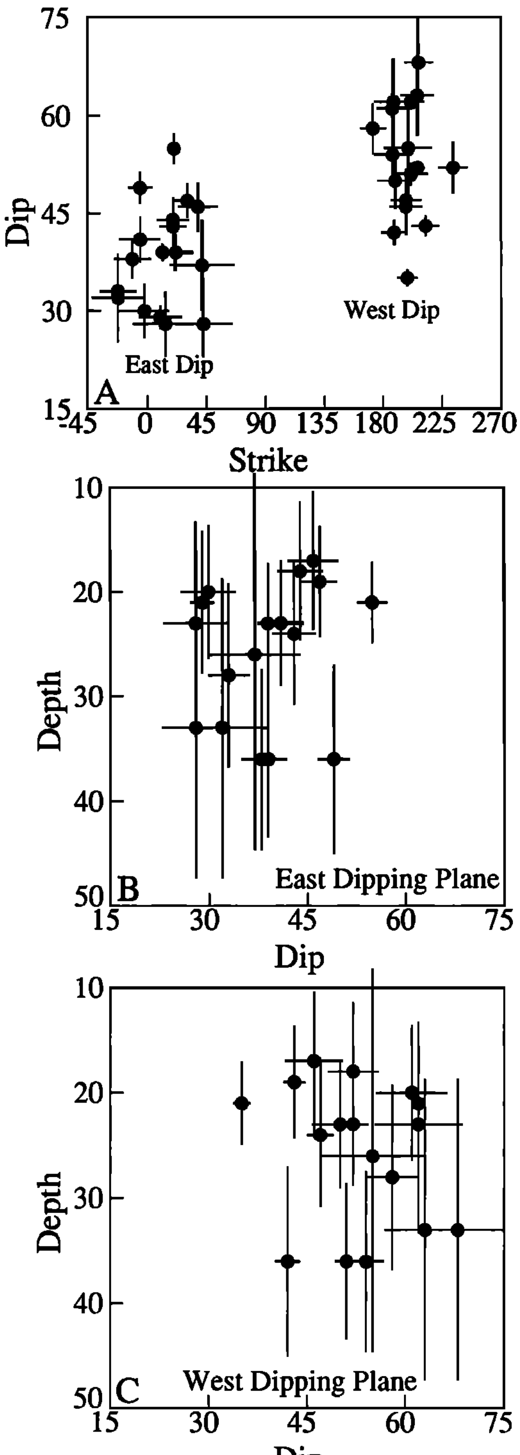

Fig. 7. (a) Plot of the dips of the nodal planes versus their strikes (the notation is such that while facing the strike direction, the plane dips to the observer's right). The east dipping plane has a strike of 19±16° and dip of 40±9° and the west dipping plane has a strike of 199±13° and dip of 53±9°. (b and c) Plots of the dip angle versus depth (in kilometers) for the east and west dipping nodal planes.

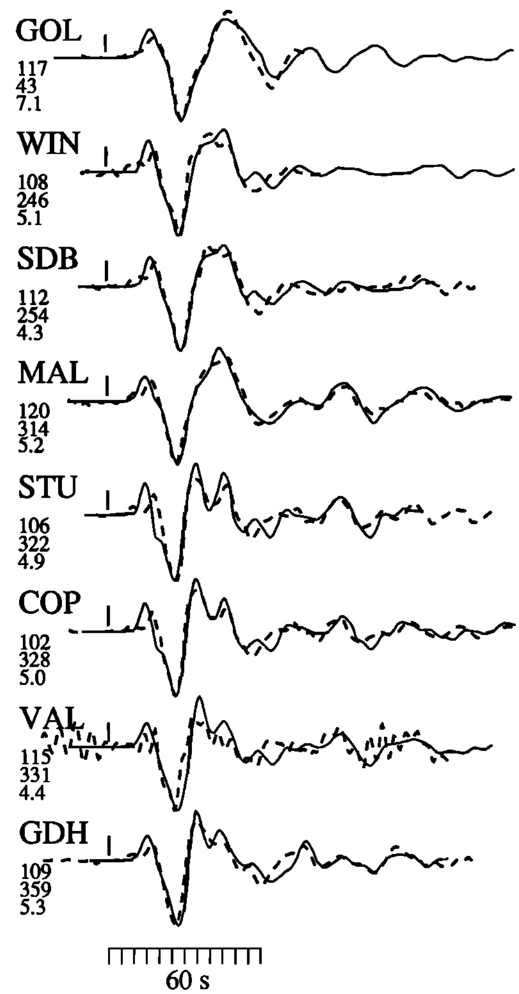

Fig. 8. Long-period WWSSN P_{dif} waveforms for the 10 August 1968 (solid lines) and 5 August 1969 (dashed lines) earthquakes superimposed. Waveforms are aligned using the ISC origin time and assuming that the travel times from both events to the station are the same. Amplitudes are normalized by their maxima, and the ratios of the maximum amplitudes (1968 over 1969) are shown as the third number below the station code. The other numbers are the distance and azimuth of the station from the epicenter, both in degrees.

seismograms at MAT and CTA that are similar in shape but slightly larger than those for 14 December 1978 (event 13) so its M_o is estimated at 10^{18} N m.

Assigning a 20% uncertainty to the moments determined by waveform and CMT analyses as well as to those just discussed and a factor of 2 uncertainty for the 10 August 1968 event, the total moment for the $m_b \geq 6.0$ earthquakes is 8.3×10^{20} N m (low = 5.2×10^{20} N m; high = 13.9×10^{20} N m). 60% of the moment is contributed by the 1968 event and 27% by the event of 14 August 1986. The total moment for shallow Molucca Sea earthquakes for the period 1964-1986 is then approximately 9.3×10^{20} N m (low=5.5×10^{20} N m; high=17.1×10^{20} N m). By the estimates above, moment contributed by earthquakes for which

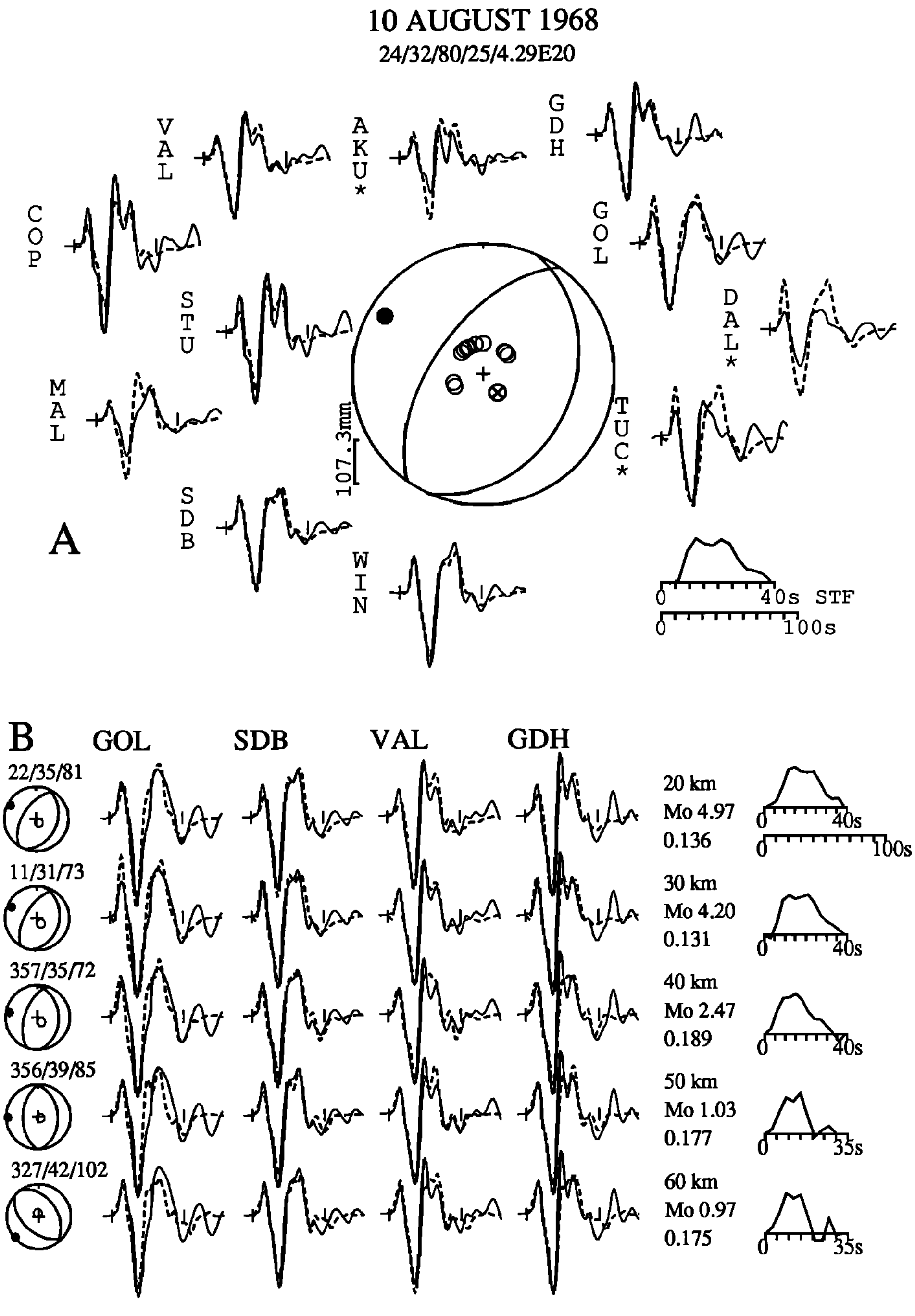

Fig. 9. (a) Minimum variance solution for the 10 August 1968 earthquake using P_{dif} waveforms. Layout as in Figure 3. All seismograms are from WWSSN instruments. The seismograms at DAL, TUC, and AKU were not used here (unweighted) because they could not be digitized for the 5 August 1969 event. (b) Selected P_{dif} waveforms and corresponding synthetics for source depth ranges of 20 to 60 km in steps of 10 km. At each depth the mechanism and source time function were allowed to vary to minimize variance of the residuals using all of the weighted seismograms shown in Figure 9a. The mechanisms are shown in the focal spheres at the left with strike, dip, and slip angles separated by slashes. At the right are the source time functions. To the left of the source time functions are the depth in kilometers, the seismic moment M_0 in 10^{20} N m, and the ratio of the variances of the amplitude residuals to the amplitudes. For the minimum variance solution at 25 km depth in Figure 9a this ratio is 0.111.

there are no fault plane solutions is approximately $5x10^{19}$ N m, or about 5% of the total.

To estimate the seismic deformation rates v_{ij} in a region where earthquakes occur on several faults of varying orientations, the elements of the moment tensor M_{ij} for each earthquake can be calculated and summed [Aki and Richards, 1980; Jackson and McKenzie, 1988; Kostrov, 1974]. Using the method of Kostrov [1974]

$$v_{ij} = l_j \Sigma M_{ij} / 2 \mu V t \tag{3}$$

where l_i is the length of the region in the i^{th} direction, $V=l_x l_y l_z$ is the volume of the region, μ is the shear modulus ($\mu = \rho V_s^2 = 4x10^{10}$ N/m^2 for the crust or $7x10^{10}$ N/m^2 for the mantle), and t is time. In the coordinate system chosen (x is parallel to the long axis of the box (N23°E) and to the TMR, y is perpendicular to the long axis of the box, and z is down), ΣM_{xx} is less than 5% of the maximum element of ΣM_{ij}. The moment tensors for all CMT and waveform solutions for events within the box were summed (Table 2). Using the length of the seismically active region beneath the TMR (Figure 2a) for l_x (250 km), its width for l_y (70 km), and the thickness of the seismogenic zone estimated from waveform solutions and microearthquake activity for l_z (25 km), the strain rates and relative velocities of rigid blocks bounding the deforming region are listed in Table 2. The minimum values for the velocities v_{ij} in Table 2 include an increase in the thickness of the seismogenic region to 40 km, to allow for uncertainties in the depths (10 to 50 km).

The rate of ESE-WNW shortening of the deforming region is given by v_{yy} = 35 mm/yr (range of 14 to 59 mm/yr). The absence of the Philippine Trench east of Halmahera suggests that Halmahera is part of the Philippine Sea plate and hence that the Molucca Sea is part of the boundary between the Eurasian and Philippine plates. At the latitude of the Molucca Sea the convergence vector between these plates is in the azimuth 114° (perpendicular to the long side of the box) with a rate of 93 mm/yr [Seno et al., 1987]. The Eurasia-Pacific vectors of Minster and Jordan [1978] (103° azimuth and 99 mm/yr rate) and DeMets et al. [1990] (106° azimuth and 92 mm/yr) are similar. Hence the seismic deformation within the Molucca Sea can account for 15% to 63% of the Eurasia-Philippine convergence.

In regions where plate motion rates are reasonably well known from independent constraints the calculated seismic deformation rates tend to be small, typically less than 10% but reaching 50% of the predicted rates [Jackson and McKenzie, 1988; Ekström and England, 1989]. Even though the rates are often much too small, the directions of the principal strains inferred from earthquake solutions are largely in accord with plate motion directions. The rate of convergence of the SE side of the deforming region with respect to the NW side is v_{yy} and the relatively small value for v_{xx} indicates that v_{yy} is nearly parallel to the direction of maximum horizontal shortening. This direction is nearly parallel to the predicted direction of Eurasia-Philippine Sea convergence. It is likely then that at its latitude the Molucca Sea forms the main boundary between the Eurasian and Philippine Sea plates.

The calculated rate of present crustal thickening (v_{zz}) is 7 to 20 mm/yr with a best estimate of 12 mm/yr; this is equivalent to 12 km/m.y. for an area 250 km long by 70 km wide. If the crustal thickening is accompanied by isostatic adjustment, then the rate of uplift h with respect to a gravitational equipotential surface of the Earth (such as sea level) is

$$h = v_{zz} (\rho_m - \rho_c) / (\rho_m - \rho_w) \tag{4}$$

where ρ_m, ρ_c, and ρ_w are the densities of the mantle, crust (including collision complex), and seawater, respectively. For assumed densities of ρ_w = 1030 kg/m^3, ρ_c = 2600 kg/m^3, and ρ_m = 3300 kg/m^3, h is roughly 30% of the thickening rate v_{zz} or about 2-6 km/m.y.

INTERPRETATION

Uplift and Emplacement of the Molucca Sea Ophiolite

A problem that has come with the interpretation of ophiolites as pieces of oceanic crust and mantle is the matter of emplacing them on land [e.g., Dewey, 1976]. Because ophiolites are dense, they must be emplaced on low-density crust in order to reach elevations above sea level and remain there.

The predominance of reverse faulting beneath the TMR suggests that active thrusting elevates the ophiolite with respect to the collision complex and sea level. The distribution of hypocenters in cross section does not define a planar feature that would provide the sense of thrusting but structure beneath the TMR suggests that the fault system dips to the west. If so, then the dips of the faults are steep (45°-60°), and the hanging wall block is quite thick. Even if the fault system dips to the east, it must do so at an angle greater than 30°. Most ophiolites, when their original thicknesses are reconstructed, are thought to be less than 12 km thick and emplaced along gently dipping faults [Coleman, 1977]. The thick Papuan ophiolite is bounded by steeply dipping faults, but these are considered secondary faults [Davies, 1971] rather than the faults along which the ophiolite was originally lifted.

In the Molucca Sea the ophiolite is currently becoming embedded in an enormous volume of low-density deformed rocks, the collision complex, by thrust faulting. Subsequent isostatic adjustment to the thickening of the collision complex will lift the ophiolite to an elevation above the flanks of the island arcs. Collapse of the central ridge under the force of gravity emplaces the ophiolite on the island arcs [Silver and Moore, 1978], and accompanying normal faulting may serve to thin the ophiolite. The free air gravity anomaly of up to -250 mGals indicates that the crust of the collision zone must rise a few more kilometers to reach isostatic equilibrium. Because the ophiolitic rocks are embedded in the collision complex, this rise will lift them well above sea level in many places.

Implications for Associated Metamorphic Rocks

Ophiolites are commonly associated with amphibolite and greenschist facies metamorphic rocks in a thin layer at their base. Young oceanic crust will have high temperatures at shallow depths where shear strain may concentrate and a detachment surface can form [Williams and Smyth, 1973]. A high geothermal gradient will increase the advective heat transfer for a given rate of vertical movement during thrusting so that the lower plate rocks will be exposed to rapid heating. Such reasoning has led to the idea that many ophiolites are emplaced hot and therefore that emplacement must occur near an oceanic

TABLE 2. Results of Summing Moment Tensors for Molucca Sea Earthquakes

Date	M_o	Strike, deg	Dip, deg	Rake, deg	M_{xx}	M_{xy}	M_{xz}	M_{yy}	M_{yz}	M_{zz}
66 3 8[1]	2.48	31	47	88	-0.07	0.40	-0.03	-2.41	-0.18	2.47
68 810	500.00	24	32	80	-1.74	53.70	-77.39	-440.83	214.54	442.57
68 811	1.00	14	60	95	-0.04	-0.21	-0.03	-0.82	-0.50	0.86
68 817	1.85	202	62	96	-0.01	-0.20	-0.07	-1.52	1.03	1.53
681031	1.63	188	61	95	-0.15	-0.45	0.16	-1.22	0.85	1.38
69 125	1.77	20	43	92	-0.01	-0.13	0.05	-1.76	0.12	1.76
69 8 5	65.00	355	49	81	-7.65	-22.06	-10.08	-55.92	-4.76	63.57
691214	3.00	178	68	173	-2.16	-1.87	-0.90	1.91	0.71	0.25
73 318	10.50	349	38	74	-1.41	-3.87	-0.53	-8.38	3.30	9.79
74 511	2.39	22	39	90	-0.00	-0.04	0.01	-2.34	0.50	2.34
75 513	7.91	21	55	91	-0.02	-0.37	-0.02	-7.41	-2.71	7.43
77 216	1.29	61	35	124	0.02	0.39	0.24	-1.02	0.65	1.00
77 7 3	2.62	190	50	100	-0.28	-0.87	-0.18	-2.26	0.50	2.54
78 7 8	1.08	168	27	50	0.08	-0.21	0.23	-0.75	-0.75	0.67
791022	6.72	173	58	98	-2.18	-2.99	1.03	-3.80	2.77	5.98
84 723	2.10	189	62	87	-0.06	-0.32	0.33	-1.68	1.13	1.74
841026	1.75	234	52	113	0.06	0.44	-0.56	-1.63	0.12	1.56
85 413	42.20	12	39	78	0.60	-2.44	-5.06	40.97	9.73	40.38
86 7 9	15.72	9	39	71	0.66	-0.57	-3.11	-15.20	3.96	14.54
86 814	226.10	347	16	34	25.99	-15.89	-82.75	-92.99	192.65	67.00
86 815	2.67	237	11	-68	0.11	-0.36	-0.47	0.81	2.45	-0.93
86 816	5.11	205	11	-94	0.01	-0.13	-0.51	1.90	4.71	-1.91
86 816	1.37	217	11	-147	0.12	-0.26	-1.26	0.16	0.40	-0.28
87 129	4.62	358	45	58	0.63	-0.39	-1.57	-4.54	0.73	3.91
87 2 8	2.46	337	48	25	1.12	-0.58	-1.12	-2.16	1.00	1.04
87 213	13.87	18	42	83	0.09	-0.07	-1.13	-13.78	1.54	13.69
87 216	2.42	213	39	89	-0.08	0.43	0.12	-2.29	-0.49	2.37
87 318	1.49	20	34	78	0.01	0.10	-0.23	-1.37	0.56	1.36
	ΣM_o	10^{18} N m			28.9	-10.1	-240.1	-771.2	564.8	742.2
	ΣM_o rate	10^{18} N m/yr			1.2	-0.4	-9.6	-30.8	22.6	29.7
	Strain rate	10^{-9}/yr			18.9	-6.6	-157.2	-504.9	369.8	485.9
	Omitting 68.8.10 and 86.8.14									
	ΣM_o	10^{18} N m			-10.5	-38.6	-31.7	-183.1	45.3	193.6
	ΣM_o rate	10^{18} N m/yr			-0.4	-1.5	-1.3	-7.3	1.8	7.7
	Strain rate	10^{-9}/yr			-6.9	-25.3	-20.7	-119.9	29.6	126.7

Velocities, mm/yr

	v_{xx}	v_{xy}	v_{xz}	v_{yx}	v_{yy}	v_{yz}	v_{zx}	v_{zy}	v_{zz}
Minimum	2.4	-0.7	-2.8	-2.5	-13.9	6.4	-17.3	11.1	7.5
Mean	4.7	-0.5	-3.9	-1.6	-35.3	9.2	-39.3	25.9	12.1
Maximum	5.4	1.4	-5.7	5.1	-58.6	13.9	-57.2	38.9	20.4
Omitting 68.8.10 and 86.8.14									
Mean	-1.7	-1.8	-0.5	-6.3	-8.4	0.7	-5.2	2.1	3.2

Only those for which CMT, waveform, or first motion solutions have been found are used. Only those events with seismic moment in excess of 10^{18} N m are listed, but all 62 events went into the summation. The minimum v_{ij} values are computed with a seismogenic layer thickness of 40 km. All moment values are in 10^{18} N m. Negative values correspond to compressive strains.

[1]Read as March 8, 1966.

spreading center. In this section I argue that the Molucca Sea provides a setting in which at least amphibolite grade metamorphic rocks can be formed at the base of a thick ophiolite emplaced long after its formation. The age of the Molucca Sea lithosphere is unknown, but the nearby portion of the Philippine Basin to the east is thought to be Eocene based on magnetic lineations, while ODP sites 767 and 770 have confirmed a middle Eocene age for the Celebes Sea to the west [Silver and Rangin, 1989]. The Molucca Sea is probably of similar age.

Pressure. Lithostatic pressure at 15 km depth at the base of the collision complex is approximately 370 MPa (3.7 kbar), using a density of the 2500 kg/m^3 for the collision complex. Where the ophiolite first thrusts over the collision complex at depth the pressure may be higher (≈460 MPa) due to the more dense (average density ≈3100 kg/m^3) overlying oceanic crust and mantle. In either case, pressure will be high enough to produce amphibolite facies metamorphism but too low for blueschist metamorphism at the likely temperatures. Tectonic stress contributes to the pressure but there is no useful constraint on this number.

Temperature. Temperatures of the collision complex where it contacts the ophiolite may also be high enough to reach amphibolite facies conditions. Reported values of heat flow in the Molucca Sea are 34 to 42 x10^{-3} W/m^2 (Lamont-Doherty Geological Observatory database). These are roughly 50% lower than global averages but are within the range of normal surface heat flow for Eocene age oceanic lithosphere and very close to the mantle-derived heat flow for crust that has reached steady state [Sclater et al., 1980]. In the Molucca Sea, heat flow produces a high surface geothermal gradient (40°-50°C/km) due to low thermal conductivity of the collision complex. Assuming steady state heat conduction (in the absence of underthrusting) and no radiogenic heat production in the collision complex, linear extrapolation of this surface gradient to 15 km depth suggests temperatures of 520°-650°C, which places the P-T conditions in the range of amphibolite to greenschist facies metamorphism.

Certainly the thermal structure of the collision complex is not so simple. Thermal modeling suggests that inverted thermal gradients and low temperatures can occur in accretionary prisms due to the steady underthrusting of cold crustal material [e.g., Wang and Shi, 1984]. Such models are not directly applicable to but can be used as a starting point for estimating the thermal structure beneath the Molucca Sea because it has been some time since the accretionary prisms collided and buried the last of the oceanic lithosphere. Typical arc-trench gaps for Pacific oceanic island arcs are 200 km, suggesting that when the trenches of the Sangihe and Halmahera arcs first collided, the volcanic arcs were likely separated by about 400 km. Now they are 150 km closer; this amount of closure would take about 2 m.y. at a rate of 75 km/m.y. Starting with a typical steady state temperature profile in an accretionary prism from Wang and Shi [1984; Figure 2] and using reasonable values for radiogenic heat production in the collision complex (8x10^{-10} W/kg) and basal heat flux (42x10^{-3} W/m^2), after 2 m.y. of thermal relaxation (in one dimension) the temperature at the base of the collision complex at 15 km depth would still be less than 300°C.

However, upthrusting of the ophilite will increase the temperature near the fault at a particular depth by lifting the deeper, warmer oceanic crust and mantle and by shear heating on the fault. Just considering shear heating, the change in temperature ΔT at the fault caused by thrusting is

$$\Delta T = \tau v\ (\kappa t/\pi)^{1/2}/K \tag{5}$$

where τ is the shear stress on the fault, v is the slip rate, κ is the diffusivity (10^{-6} m^2/s), t is time, and K is the thermal conductivity (2 W/m °K) [Molnar and England, 1990]. In this equation it is implicit that the heat generated is split evenly between the hanging and foot walls. Under the constraints that the shear stress is less than 100 MPa and that the total displacement (vt) is no more than the downdip length of the fault (40 km; i.e., set t=40 km/v), any slip rate of 40 mm/yr or greater will raise the temperature at the fault by more than 200°C.

The slip rate v is estimated from the seismic moments of the earthquakes using the Brune [1968] relationship $v = \Sigma M_o/\mu A t_s$, where μ is the shear modulus, A is the fault area, and t_s is the time during which the earthquakes occurred (24 years). Assuming that the the fault dips 45°, so that its downdip length is 40 km, and that its length is 250 km, the area A=10^{10} m^2. ΣM_o=9x10^{20} N m from above so that v=54 to 90 mm/yr. For this range of slip rates the shear stress needed to raise the temperature at the fault by 200°C after 40 km of thrusting ranges from 85 to 66 MPa, which is probably a reasonable range [e.g., Molnar and England, 1990].

Under these conditions the rocks may reach temperatures high enough to induce amphibolite metamorphism in them, and these rocks may be pulled to the surface with the ophiolite. A similar mechanism for the development and transport of the amphibolite rocks beneath ophiolites in Oman [Ghent and Stout, 1981] and Newfoundland [Coleman, 1977] has been suggested. The thinness of the metamorphic zone is attributed to tectonic thinning by shearing during emplacement. The Molucca Sea thus provides a possible modern setting for the rapid ascent by high-angle thrust faulting of metamorphic rocks beneath an ophiolite.

FAVORABLE CONDITIONS IN THE MOLUCCA SEA FOR THE EMPLACEMENT OF AN OPHIOLITE

When compared to the amount of oceanic crust that has been subducted, the amount that has been emplaced on land as ophiolites is exceedingly small; it is estimated at less than 0.001% [Coleman, 1977]. It is clear that no single set of circumstances can be used to explain the emplacement (obduction) of all known ophiolites [Dewey, 1976]. Therefore one can conclude that it takes one of multiple special sets of circumstances to bring about the exposure of ophiolite on land. The tectonic setting of the Molucca Sea provides one of these uncommon situations and so the following question is addressed: What in particular within this setting causes oceanic crust to be detached and uplifted rather than being subducted? The favored interpretation developed in the following is that the concave down shape of the Molucca Sea lithosphere prevents it from sinking fast enough to avoid colliding with the approaching island arcs, allowing some crust and upper mantle to be stripped from it by thrust faulting.

Source of Deviatoric Stress in the Molucca Sea Lithosphere

A first important point to establish is that the deformation of the Molucca Sea lithosphere is caused by it being squeezed between the two converging island arcs. This provides the work required to lift the ophiolite against gravity. Two lines of evidence suggest that the stress causing deformation in the Molucca Sea lithosphere is largely due to plate convergence. One is the presence of thrust faulting at all depths beneath the TMR despite the strong bending of the lithosphere, and the second is that in the backarcs behind both the Sangihe and Halmahera arcs, thrust zones are develping. One may be tempted to interpret the strongly negative gravity field of the Molucca Sea as evidence of compressive stress, but this may also arise by flexing the lithosphere by loading from above (the overthrust island arcs) and below (slabs pulling).

The lithosphere beneath the Molucca Sea is bent into a concave down shape in cross section, as defined by earthquake hypocenters [e.g., Cardwell et al., 1980]. Elastic plate bending theory and observations of earthquakes at trenches suggest that bending of the lithosphere leads to tensional deviatoric stress in its upper part (normal faulting) and compression (thrust faulting) in its lower part [e.g., Chapple and Forsyth, 1979]. Tectonic stress will shift the depth of the transition from normal to thrust faulting. Thrust faulting beneath the TMR occurs throughout the seismogenic layer of the plate (Figure 5b) arguing that a strong compressive tectonic stress perpendicular to the TMR acts on the Molucca Sea lithosphere. Figure 2b shows a few small normal faulting mechanisms, but these are atypical mechanisms for bending earthquakes (i.e., one very steep and one gently dipping nodal plane).

The second piece of evidence is the presence of thrusting (compression) along both the eastern and western margins of the collision zone (i.e., at the Cotabato and Philippine trenches). This suggests that the Philippine and Eurasian plates converge faster than the arcs do. It follows then that the two island arcs are being driven together by convergence of the Eurasian and Philippine plates rather than being pulled together by the sinking Molucca Sea lithosphere.

Accommodation of Lithospheric Thickening in the Collision Zone

Given that the rate at which the island arcs converge is determined by plate motions and not by how fast the Molucca Sea lithosphere can sink, we now ask if the Molucca Sea lithosphere can sink fast enough to avoid getting caught in the deformation of the collision zone? The influx of island arc material thickens the lithosphere of the collision zone at a rate of vH/L, where where v is the convergence rate between the two arcs, H is the thickness of the incoming plates, and L is the width of the collision zone, the distance from one arc to the other. Taking maximum values of H at 100 km, of L at 250 km, and of v at the convergence rate between Eurasia and the Philippine Sea plate (90 km/m.y.), the thickening rate is at most 36 km/m.y.

Thickening the collision zone will increase the load on the Molucca Sea lithosphere, and it will sink as the viscous upper mantle flows in response. Ignoring the flexural strength of the lithosphere for long-wavelength loads and treating the underlying asthenosphere as a viscous half-space, I assume for simplicity that the two-dimensional load on the upper boundary of the asthenosphere is of the form $w_o = A \cos 2\pi x/\lambda$ where A is the maximum amplitude and λ is the wavelength of the load. In this formulation, w_o is the thickness of a load of the same density as the viscous fluid representing the asthenosphere. The load w_o can also be expressed as the thickness of a load with density ρ_l by multiplying it by ρ_l/ρ_a, where ρ_a is the density of the fluid (i.e., the upper asthenosphere; $\rho_a \approx 3400$ kg/m^3).

In response to a load w_o the height w of the upper boundary of the viscous half-space after a time t at any point is

$$w(t) = w_o \exp(-\rho_a g \lambda t/4\pi\mu) \tag{6}$$

where g is the acceleration of gravity (9.8 m/s^2) and μ is the viscosity of the asthenosphere (10^{21} Pa s) [Turcotte and Schubert, 1982]. At a peak in the initial load w_o (at x=0 where w_o=A) the system will reach steady state when the rate of lithospheric thickening equals negative the rate of sinking:

$$vH/L\ \rho_l/\rho_a = -dw/dt = A/\tau_r\ \exp(-t/\tau_r) \tag{7}$$

where $\tau_r = 4\pi\mu/\lambda\rho_a g$. We want to know the value of the load amplitude A_e at which the instantaneous rate of sinking equals the rate of thickening estimated earlier. Setting t=0 and solving for A_e

$$A_e = \tau_r vH\rho_l/L\rho_a \tag{8}$$

Using λ = 250 km and ρ_l=3100 kg/m^3, we get τ_r = 0.05 m.y. and $A_e \approx 1570$ m. The thickness A_e for an equivalent load of collision complex with density $\rho_{cc} \approx 2500$ kg/m^3 (multiply by ρ_l/ρ_{cc}) is less than 2000 m. This means that for a 36 mm/yr increase in thickness of a load with a wavelength of the width of the Molucca Sea, the asthenosphere will flow fast enough to accommodate the increase after only 2 km of collision complex is present. The Molucca Sea has certainly exceeded this condition, and so I conclude that for the half-space geometry assumed above, the Molucca Sea lithosphere can easily sink fast enough to avoid being caught between the island arcs.

The foregoing analysis presumes unrestricted flow in an asthenospheric half-space. The normal flow in the asthenosphere for a load with the wavelength of the Molucca Sea collision zone is most important in the upper 150 km (Figure 10). However, beneath the Molucca Sea the subducted slabs extend to at least this depth beneath both arcs and truncate such a flow pattern. Based on common sense rather than continued analysis, I suggest that the concave down shape of the lithosphere beneath the Molucca Sea inhibits the flow in the asthenosphere that is necessary for the lithosphere to sink. In this sense the subducted slabs act like a parachute that decreases the rate of descent of its load. Because the slab beneath the Halmahera arc extends only a few hundred kilometers along strike, lateral flow parallel to the slabs may play a role but still the resistance to sinking is likely greater than that in the absence of such slabs. Slowing the plate's sinking keeps it at relatively shallow depth within the collision zone with the consequence that the island arcs squeeze the lithosphere and thrust faulting detaches blocks of ophiolite.

SOME TECTONIC SETTINGS FOR OPHIOLITE EMPLACEMENT

I have suggested that the concave down shape of the Molucca Sea lithosphere increases its resistance to sinking; in a sense this decreases the effective negative buoyancy of the oceanic litho-

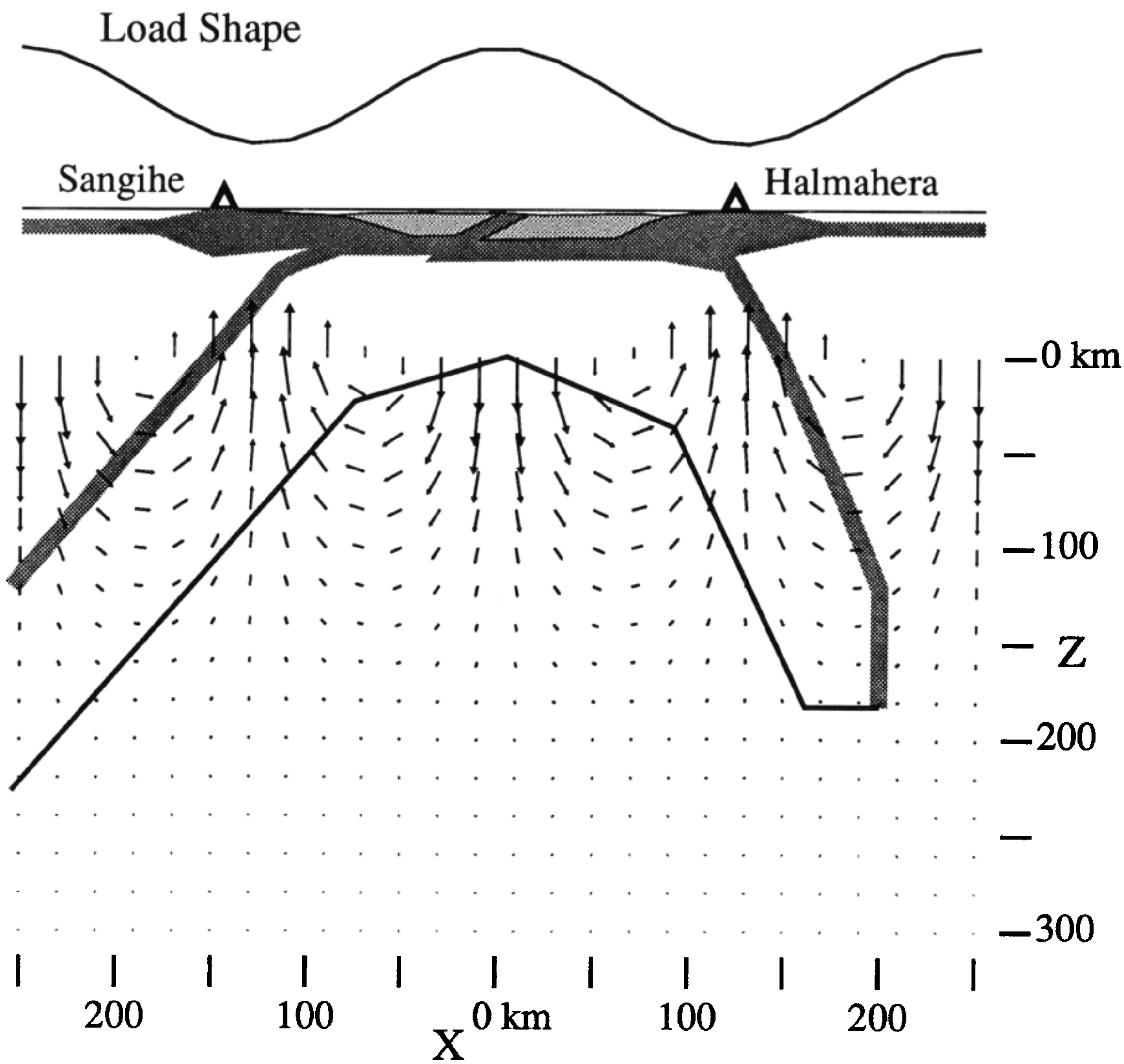

Fig. 10. Cross section of the Molucca Sea region showing the expected flow pattern in the asthenosphere for a sinusoidal surface load, $w_o = A \cos 2\pi x/\lambda$ (shown at top). Here λ=250 km. The flow vectors are calculated from equations 6-91 and 6-92 of Turcotte and Schubert [1982]. Vector lengths are proportional to velocity but are scaled arbitrarily. Superimposed on the flow pattern is the outline of the crustal model from McCaffrey et al. [1980] and lithospheric slabs as estimated by earthquake foci. Heavy stippling is island arc and oceanic crust, and light stippling is collision complex. All distances are in kilometers with no vertical exaggeration (the depth scale starts at the top of the asthenosphere).

sphere. In general, continental crust will deform rather than subduct in thrust belts for a similar reason; i.e., because its positive buoyancy prevents it from sinking into the mantle. In continental thrust belts the ductile lower continental crust allows detachment of sheets of upper crust. In a similar setting involving oceanic lithosphere, the detachment will likely form in the upper mantle where the increase in temperature with depth lowers strength, and the thrust sheets may comprise complete ophiolites.

Assuming that the critical factor in the Molucca Sea is the inability of the lithosphere to sink fast enough to escape the converging island arcs, other possible tectonic settings in which ophiolites are detached and emplaced may be identified by a similar inability of the oceanic lithosphere to sink. A setting that has been suggested by numerous geologists from the association of some ophiolites with high-temperature, low-pressure metamorphic rocks and the young emplacement age of ophiolites is near a spreading ridge. I suggest that part of the reason that subduction of a spreading ridge is a likely setting for ophiolite obduction is that the slab pull force may be greatly reduced if the subducted portion of the slab is young and warm and with a density not much greater than that of ambient mantle rocks.

Figure 11 shows two examples where restricted flow in the asthenosphere due to the presence of two subducted slabs may inhibit subduction. In Figure 11a, if the subduction zone on the left is active (with or without the one on the right being active), then asthenosphere will have to flow out of the region between the slabs if the material is incompressible. As the slabs approach one another this flow will be severely restricted and prevent further subduction of the slab(s). Figure 11b shows a slab thrusting from the backarc and isolating the asthenosphere above the subducting plate. Depending on how the slabs sink with respect to the mantle, the restriction of flow in the asthenosphere above the subducting plate may inhibit the sinking of the slab.

Continental collisions often emplace ophiolites in the final stages of ocean closure, so I attempt to explain ophiolite emplacement at continent collisions in terms of this idea of inhibited subduction. Two factors may contribute to the slowing of subduction of the oceanic lithosphere leading the passive continental margin just prior to a collision between continents or between a passive continental margin and an island arc. First I assume that continental lithosphere, because of its thick, low-density crust, is positively buoyant with respect to the mantle so tends to resist subduction. Also the continental lithosphere may have a greater flexural rigidity than the oceanic lithosphere in front if it [e.g., Watts et al., 1980] and so requires additional force to cause it to bend into the trench. Because of these factors, once the continental lithosphere begins to bend downward as it approaches a trench, an increasing amount of force (e.g., slab pull) is required to maintain the trench profile. In other words, the buoyancy and rigidity of the continental crust exert a force that tends to pull up on the subducting lithosphere, which at this point is oceanic below the trench and accretionary prism (Figures 11c and 11d). The relative magnitudes of these opposing forces are not usefully constrained, so this suggestion is qualitative at best.

Drawing from the Molucca Sea example, the development of a concave down pocket of asthenosphere beneath the continental margin (Figures 11c and 11d) may act to inhibit subduction. The source of the thicker nonconvecting layer beneath the continent is speculative but may correspond to a thicker thermal boundary layer for continents than for oceans [Sclater and Francheteau, 1970]. The nonconvecting layer beneath the continents may be even thicker according to Jordan's [1975] concept of a continental tectosphere, which would serve to increase both the extent of the pocket and the resistance to sinking.

CONCLUSIONS

Earthquakes indicate that high-angle (dips of 30°-60°) thrust faulting beneath the Talaud-Mayu Ridge in the central Molucca Sea penetrates at least 15 km into the upper mantle and acts to elevate pieces of the crust and upper mantle at a rapid rate. These pieces likely include thick ophiolites detached from the Molucca Sea lithosphere. The high level of seismic activity beneath the Molucca Sea is consistent with it accommodating a large part of Philippine-Eurasian convergence. Rapid slip rates on the thrust faults may generate enough heat so that hanging

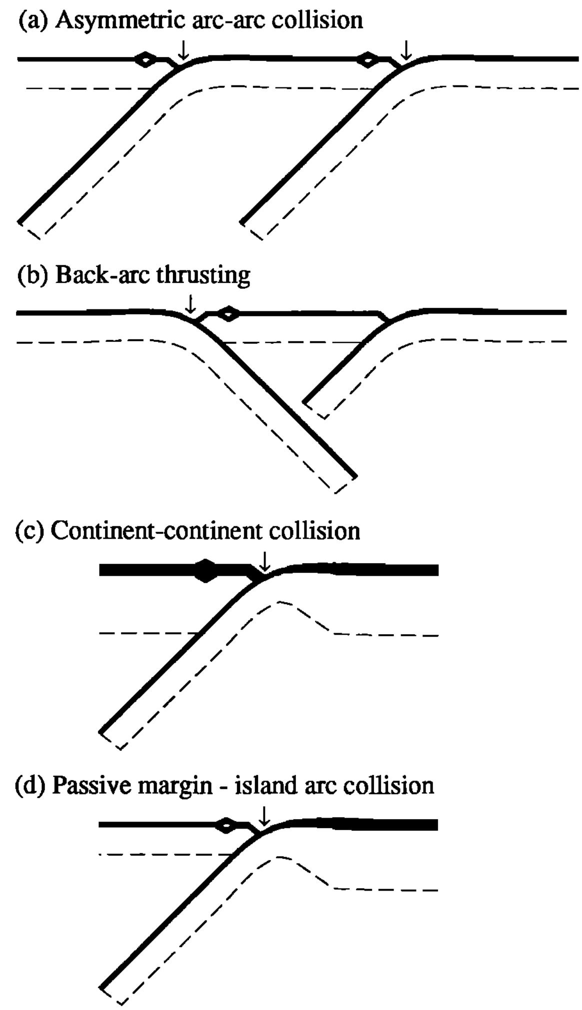

Fig. 11. Hypothetical situations in which the asthenospheric flow below or above a subducting slab can be inhibited causing the slab to sink more slowly than it would under normal conditions. If the lithosphere cannot sink it will get caught up in the surface compressional tectonics and pieces of its crust and upper mantle may be detached and thrust over the leading edge of the upper plate (likely sites for ophiolite detachment are shown by the arrows). Heavy lines represent crust, open diamonds represent oceanic island arcs, and solid diamonds are continental arcs. Trenches are exaggerated for clarity. The dashed lines represent rapid changes in the mechanical properties of the mantle which, under the oceans, is the base of the lithosphere. For this figure the significance of this line is that it separates the convecting lower portion of the mantle from the upper part that stays with the plate. (a) In an asymmetric arc-arc collision the presence of two slabs restricts the flow of asthenosphere between them in such a way that one or both of the subducting slabs are slowed. (b) The asthenosphere beneath the upper plate may be isolated by the slab subducting from a backarc basin. (c and d) Under the continents the mechanical boundary may be thicker than beneath the oceans and produce a concave down pocket of asthenosphere, similar to the case in the Molucca Sea.

wall rocks below the ophiolite reach temperatures for amphibolite facies metamorphism, and these metamorphic rocks may be pulled to the surface with the ophiolite. The convergence of the Philippine and Eurasian plates provides the energy necessary to lift the ophiolite above sea level.

The Molucca Sea collision zone provides a suitable setting for the detachment and uplift of ophiolites because the concave down shape of the subducting lithosphere slows its rate of sinking, thereby trapping the oceanic lithosphere in the collision zone instead of allowing it to sink out of the way. This suggests that tectonic situations for ophiolite emplacement may arise when the subducting oceanic lithosphere is buoyed up at the trench. Such situations may occur when subduction of young, low-density oceanic lithosphere near a spreading ridge decreases the slab pull, when the onset of subduction of low-density and perhaps more rigid continental lithosphere resists subduction, or when the flow in the asthenosphere necessary to allow the lithosphere to sink is geometrically confined and thereby restricted.

Acknowledgments. This work was supported by National Science Foundation grant EAR84-20860. I thank Frank Spear for helpful discussions, Greg Moore for his review, and Geoff Abers for help in gathering data.

REFERENCES

Abers, G. A., Active tectonics and seismicity of New Guinea, Ph.D. thesis, Mass. Inst. of Technol., Cambridge, 1989.

Aki, K., and P. G. Richards, *Quantitative Seismology, Theory and Methods*, 557 pp., W. H. Freeman, San Francisco,, 1980.

Brune, J. N., Seismic moment, seismicity, and rate of slip along major fault zones, *J. Geophys. Res., 73*, 777-784, 1968.

Cardwell, R. K., B. L. Isacks, and D. E. Karig, The spatial distribution of earthquakes, focal mechanism solutions, and subducted lithosphere in the Philippine and northeastern Indonesian islands, in *The Tectonic and Geologic Evolution of Southeast Asian Sea and Islands, Geophys. Monogr. Ser.*, vol. 23, edited by D. E. Hayes, pp. 1-35, AGU, Washington, D. C., 1980.

Chapple, W. M., and D. W. Forsyth, Earthquakes and bending of plates at trenches, *J. Geophys. Res., 84*, 6729-6749, 1979.

Christensen, N. I., and M. H. Salisbury, Structure and constitution of the lower oceanic crust, *Rev. Geophys. Space Phys., 13*, 57-86, 1975.

Coleman, R. G., *Ophiolites*, 229 pp., Springer-Verlag, New York, 1977.

Davies, H. L., Peridotite-gabbro-basalt complex in eastern Papua: An overthrust plate of oceanic mantle and crust, *Bull. Bur. Min. Resour., 128*, 48 pp., 1971.

DeMets, C., R. G. Gordon, D. F. Argus, and S. Stein, Current plate motions, *Geophys. J. Int., 101*, 425-478, 1990.

Dewey, J. F., Ophiolite obduction, *Tectonophysics, 31*, 93-120, 1976.

Dewey, J. F., and J. M. Bird, Mountain belts and the new global tectonics, *J. Geophys. Res., 75*, 2625-2647, 1970.

Dziewonski, A. M., T. -A. Chou, and J. H. Woodhouse, Determination of earthquake source parameters from waveform data for studies of global and regional seismicity, *J. Geophys. Res., 86*, 2825-2852, 1981.

Ekström, G., and A. M. Dziewonski, Evidence of bias in the estimation of earthquake size, *Nature, 332*, 319-323, 1988.

Ekström, G., and P. England, Seismic strain rates in regions of distributed continental deformation, *J. Geophys. Res., 94*, 10,231-10,257, 1989.

Ghent, E. D., and M. Z. Stout, Metamorphism at the base of the Samail ophiolite, southeastern Oman Mountains, *J. Geophys. Res., 86*, 2557-2572, 1981.

Hamilton, W., Subduction in the Indonesian region, in *Island Arcs, Deep Sea Trenches, and Back-Arc Basins, Maurice Ewing Ser.*, vol. 1, edited by M. Talwani and W. C. Pitman III, pp. 15-31, AGU, Washington, D. C., 1977.

Hamilton, W., Tectonics of the Indonesian region, *U.S. Geol. Surv. Prof. Pap. 1078*, 345 pp., 1979.

Hawkins, J. W., C. A. Evans, E. F. Wright, and G. F. Moore, East Mindanao ophiolite belt: Petrology and metamorphosed basal cumulate rocks, *Eos Trans. AGU, 62*, 1086, 1981.

Helmberger, D. V., Generalized ray theory for shear dislocation, *Bull. Seismol. Soc. Am., 64*, 45-64, 1974.

Jackson, J., and D. McKenzie, The relationship between plate motions and seismic moment tensors, and the rates of active deformation in the Mediterranean and Middle East, *Geophys. J., 93*, 45-73, 1988.

Jordan, T. H., The continental tectosphere, *Rev. Geophys. Space Phys., 13*, 1-12, 1975.

Kostrov, B. V., Seismic moment and energy of earthquakes, and seismic flow of rocks, *Izv. Acad. Sci. USSR Phys. Solid Earth, Engl. Transl., 1*, 23-44, 1974.

Langston, C. A., and D. V. Helmberger, A procedure for modeling shallow dislocation sources, *Geophys. J. R. Astron. Soc., 42*, 117-130, 1975.

McCaffrey, R., Lithospheric deformation within the Molucca Sea arc-arc collision: Evidence from shallow and intermediate earthquake activity, *J. Geophys. Res., 87*, 3663-3678, 1982.

McCaffrey, R., Active tectonics of the eastern Sunda and Banda arcs, *J. Geophys. Res., 93*, 15,163-15,182 1988.

McCaffrey, R., E. A. Silver, and R. W. Raitt, Crustal structure of the Molucca Sea collision zone, in *The Tectonic and Geologic Evolution of Southeast Asian Sea and Islands, Geophys. Monogr. Ser.*, vol. 23, edited by D. E. Hayes, pp. 161-177, AGU, Washington, D. C., 1980.

McCaffrey, R., and J. Nabelek, Seismological evidence for shallow thrusting north of the Timor trough, *Geophys. J. R. Astron. Soc., 85*, 365-381, 1986.

McCaffrey, R., and J. Nabelek, Earthquakes, gravity and the origin of the Bali Basin: An example of a nascent continental fold-and-thrust belt, *J. Geophys. Res., 92*, 441-460, 1987.

McCaffrey, R., G. A. Abers, and P. Zwick, Inversion of teleseismic body waves, *IASPEI Software Library*, vol. 3, Int. Assoc. Seismol. Phys. Earth Inter., Menlo Park, in press, 1991.

Minster, J. B., and T. H. Jordan, Present-day plate motions, *J. Geophys. Res., 83*, 5331-5354, 1978.

Molnar, P., and P. England, Temperature, heat flux, and frictional stress near major faults, *J. Geophys. Res., 95*, 4833-4856, 1990.

Moore, G. F., and E. A. Silver, Collision processes in the northern Molucca Sea, in *The Tectonic and Geologic Evolution of Southeast Asian Sea and Islands, Part 2, Geophys. Monogr. Ser.*, vol. 27, edited by D. E. Hayes, pp. 360-372, AGU, Washington, D. C., 1983.

Moore, G. F., D. Kadarisman, C. A. Evans, and J. W. Hawkins, Geology of the Talaud Islands, Molucca Sea collision zone, northeast Indonesia, *J. Struct. Geol.*, *3*, 467-475, 1981.

Moores, E. M., and H. W. Day, Overthrust model for the Sierra Nevada, *Geology*, *12*, 416-419, 1984.

Nabelek, J., Determination of earthquake source parameters from inversion of body waves, Ph.D. thesis, Mass. Inst. of Technol., Cambridge, 1984.

Nabelek, J., Geometry and mechanism of faulting of the 1980 El Asnam, Algeria, earthquake from inversion of teleseismic body waves and comparison with field observations, *J. Geophys. Res.*, *90*, 12713-12728, 1985.

Nelson, M. R., R. McCaffrey, and P. Molnar, Source parameters for 11 earthquakes in the Tien Shan, Central Asia, determined by P and SH waveform inversion, *J. Geophys. Res.*, *92*, 12629-12648, 1987.

Nichols, G., R. Hall, J. Milsom, D. Masson, L. Parson, N. Sikumbang, B. Dwiyanto, and H. Gallagher, The southern termination of the Philippine trench, *Tectonophysics*, in press, 1990.

Schweickert, R. A., and D. S. Cowan, Early Mesozoic tectonic evolution of the Western Sierra Nevada, *Geol. Soc. Am. Bull.*, *86*, 1329-1336, 1975.

Sclater, J. G., and J. Francheteau, The implications of terrestrial heat flow observations on current tectonic and geochemical models of the crust and upper mantle of the Earth, *Geophys. J. R. Astron. Soc.*, *20*, 509-542, 1970.

Sclater, J. G., C. Jaupart, and D. Galson, The heat flow through the oceanic and continental crust and the heat loss of the Earth, *Rev. Geophys. Space Phys.*, *18*, 269-311, 1980.

Seno, T., T. Moriyama, S. Stein, D. F. Woods, C. Demets, D. Argus, and R. Gordon, Redetermination of the Philippine Sea plate motion, *Eos Trans. AGU*, *68*, 1474, 1987.

Silver, E. A., and J. C. Moore, The Molucca Sea collision zone, Indonesia, *J. Geophys. Res.*, *83*, 1681-1691, 1978.

Silver, E. A., and C. Rangin, Celebes and Sulu marginal basins: Constraints from ODP Leg 124, *Eos Trans. AGU*, *70*, 1365, 1989.

Silver, E. A., and R. B. Smith, Comparison of terrane accretion in Southeast Asia and the Mesozoic North American Cordillera, *Geology*, *11*, 198-202, 1983.

Silver, E. A., R. McCaffrey, Y. Joyodiwiryo, and S. Stevens, Ophiolite emplacement by collision between the Sula Platform and the Sulawesi island arc, *J. Geophys. Res.*, *88*, 9419-9435, 1983.

Stein, S., and D. Wiens, Depth determination for teleseismic earthquakes: methods and results, *Rev. Geophys. Space Phys.*, *24*, 806-832, 1986.

Sukamto, R., Tectonic significance of melange on the Talaud Islands of northeastern Indonesia, *Bull. Geol. Res. Dev. Cent. Bandung, Indones.*, *2*, 7-19, 1979.

Turcotte, D., and G. Schubert, *Geodynamics*, 450 pp., John Wiley, New York, 1982.

Wang, C. -Y., and Y. -L. Shi, On the thermal structure of subduction complexes: A preliminary study, *J. Geophys. Res.*, *89*, 7709-7718, 1984.

Watts, A. B., J. H. Bodine, and M. S. Steckler, Observations of flexure and the state of stress in the oceanic lithosphere, *J. Geophys. Res.*, *85*, 6369-6376, 1980.

Williams, H., and W. R. Smyth, Metamorphic aureoles beneath ophiolite suites and Alpine peridotites: Tectonic implications with west Newfoundland examples, *Am. J. Sci.*, *273*, 594-621, 1973.

R. McCaffrey, Department of Geology, West Hall, Rensselaer Polytechnic Institute, Troy, NY 12180-3590.

(Received February 20, 1990;
revised November 1, 1990;
accepted November 15, 1990.)